Title

Deletion in mice of X-linked, Brugada syndrome–and atrial fibrillation–associated Kcne5 augments ventricular Kv currents and predisposes to ventricular arrhythmia

Journal

The FASEB Journal, 33(2)

ISSN

0892-6638

Authors

David, Jens-Peter
Lisewski, Ulrike
Crump, Shawn M
et al.

Publication Date

2019-02-01

DOI

10.1096/fj.201800502r

THE FASEB JOURNAL • RESEARCH • www.fasebj.org

Deletion in mice of X-linked, Brugada syndrome– and atrial fibrillation–associated *Kcne5* augments ventricular K_V currents and predisposes to ventricular arrhythmia

Jens-Peter David,[*,†,1] Ulrike Lisewski,[‡,§,1] Shawn M. Crump,[¶] Thomas A. Jepps,[*,†] Elke Bocksteins,[‖,2] Nicola Wilck,[‡,§,3] Janine Lossie,[‡,§,4] Torsten K. Roepke,[‡,§,1] Nicole Schmitt,[*,†,1] and Geoffrey W. Abbott[¶,1,5]

[*]Danish National Research Foundation Centre for Cardiac Arrhythmia and [†]Department of Biomedical Sciences, University of Copenhagen, Copenhagen, Denmark; [‡]Medical Clinic and Polyclinic for Cardiology and Angiology, and [§]Experimental and Clinical Research Center (ECRC), Charité Medical University of Berlin, Berlin, Germany; [¶]Bioelectricity Laboratory, Department of Physiology and Biophysics, University of California, Irvine, Irvine, California, USA; and [‖]Laboratory for Molecular Biophysics, Physiology, and Pharmacology, Department for Biomedical Sciences, University of Antwerp, Antwerp, Belgium

ABSTRACT: ***KCNE5*** **is an X-linked gene encoding KCNE5, an ancillary subunit to voltage-gated potassium (K_V) channels. Human *KCNE5* mutations are associated with atrial fibrillation (AF)– and Brugada syndrome (BrS)–induced cardiac arrhythmias that can arise from increased potassium current in cardiomyocytes. Seeking to establish underlying molecular mechanisms, we created and studied *Kcne5* knockout (*Kcne5*$^{-/0}$) mice. Intracardiac ECG revealed that *Kcne5* deletion caused ventricular premature beats, increased susceptibility to induction of polymorphic ventricular tachycardia (60 *vs.* 24% in *Kcne5*$^{+/0}$ mice), and 10% shorter ventricular refractory period. *Kcne5* deletion increased mean ventricular myocyte K_V current density in the apex and also in the subpopulation of septal myocytes that lack fast transient outward current ($I_{to,f}$). The current increases arose from an apex-specific increase in slow transient outward current-1 ($I_{Kslow,1}$) (conducted by K_V1.5) and $I_{to,f}$ (conducted by K_V4) and an increase in $I_{Kslow,2}$ (conducted by K_V2.1) in both apex and septum. Kcne5 protein localized to the intercalated discs in ventricular myocytes, where K_V2.1 was also detected in both *Kcne5*$^{-/0}$ and *Kcne5*$^{+/0}$ mice. In HL-1 cardiac cells and human embryonic kidney cells, KCNE5 and K_V2.1 colocalized at the cell surface, but predominantly in intracellular vesicles, suggesting that *Kcne5* deletion increases $I_{K,slow2}$ by reducing K_V2.1 intracellular sequestration. The human AF-associated mutation KCNE5-L65F negative shifted the voltage dependence of K_V2.1-KCNE5 channels, increasing their maximum current density >2-fold, whereas BrS-associated KCNE5 mutations produced more subtle negative shifts in K_V2.1 voltage dependence. The findings represent the first reported native role for Kcne5 and the first demonstrated Kcne regulation of K_V2.1 in mouse heart. Increased K_V current is a manifestation of *KCNE5* disruption that is most likely common to both mouse and human hearts, providing a plausible mechanistic basis for human *KCNE5*-linked AF and BrS.—David, J.-P., Lisewski, U., Crump, S. M., Jepps, T. A., Bocksteins, E., Wilck, N., Lossie, J., Roepke, T. K., Schmitt, N., Abbott, G. W. Deletion in mice of X-linked, Brugada syndrome– and atrial fibrillation–associated *Kcne5* augments ventricular K_V currents and predisposes to ventricular arrhythmia. FASEB J. 33, 2537–2552 (2019). www.fasebj.org**

KEY WORDS: MiRP4 · I_{Kslow} · I_{to} · potassium channel

ABBREVIATIONS: 4-AP, 4-aminopyridine; *ACTB*, β-actin; AF, atrial fibrillation; BrS, Brugada syndrome; ECG, electrocardiograph; HA, hemagglutinin; HEK, human embryonic kidney; HpTx, heteropodatoxin; ICD, intercalated disc; $I_{K,slow}$, slow transient outward current generated by K_V1.4; $I_{K,slow1}$, slow transient outward current generated by K_V1.5; $I_{K,slow2}$, slow transient outward current generated by K_V2.1; I_{ss}, steady-state current; $I_{to,s}$, slow transient outward current; $I_{to,f}$, fast transient outward current, *Kcne*, potassium voltage-gated channel, subfamily E; K_V, voltage-gated potassium channel; LAMP, lysosomal-associated membrane protein; TEA, tetraethylammonium; *TOP1*, topoisomerase-1; VPB, ventricular premature beat; VT, ventricular tachycardia; WT, wild type

[1] These authors contributed equally to this work.

[2] Current affiliation: Quality by Design NV, Wilrijk, Belgium.

[3] Current affiliation: Medizinische Klinik mit Schwerpunkt Nephrologie und Internistische Intensivmedizin Charité–Universitätsmedizin Berlin, Berlin, Germany and Experimental and Clinical Research Center (ECRC), Berlin, Germany.

[4] Current affiliation: Omeicos Therapeutics, Berlin, Germany.

[5] Correspondence: Bioelectricity Laboratory, Department of Physiology and Biophysics, Med Sci D337, School of Medicine, University of California, Irvine, Irvine, CA 92697, USA. E-mail: abbottg@uci.edu

doi: 10.1096/fj.201800502R

This article includes supplemental data. Please visit *http://www.fasebj.org* to obtain this information.

The potassium voltage-gated channel, subfamily E (KCNE) family of ion channel β subunits consists of 5 members, KCNE1–5, also called minK and minK-related peptides 1–4 respectively. They are single-pass membrane proteins with an extracellular N terminus and an intracellular C terminus and act as ancillary subunits for various voltage-gated potassium (K_V) and other channels (for reviews, see refs, 1–4). Expression profiles vary, yet all *KCNE* genes are reportedly expressed in the human heart (5–7). Likewise, all KCNE family members have been linked to cardiac arrhythmias, including atrial fibrillation (AF), Brugada syndrome (BrS), and long QT syndrome (8). Best characterized is the role of KCNE1 in the heart, where it is considered the primary β-subunit for the K_V7.1 (KCNQ1) channel in the human heart. Together, K_V7.1 and KCNE1 are thought to be the predominant molecular correlate of the slow delayed rectifier potassium current (I_{Ks}) which is a major contributor to the repolarization of human ventricular myocyte action potentials (9–11).

Whereas KCNE1-4 are relatively well studied, knowledge of the X-linked *KCNE5* (also termed *KCNE1L*) gene is limited. *KCNE5* was originally identified as one of several deleted genes in patients with the rare Alport syndrome, mental retardation, midface hypoplasia, and elliptocytosis contiguous gene syndrome characterized by a large deletion of the X chromosome (Xq22.3) (12). Notable features of the disease are Alport syndrome, mental retardation, midface hypoplasia, and elliptocytosis (13, 14). In one study, affected men show a more complex phenotype including mild abnormalities of the heart: 1 patient displayed a slow right atrial rhythm and short PR interval and also had some minor cardiac morphologic abnormalities (12). Several *KCNE5* variants are associated with AF or BrS, and different ion channels have been shown to be misregulated by the various *KCNE5* variants, including the K_V7.1 and K_V4 channels (15–17). In addition, we have demonstrated that the KCNE5 protein interacts with K_V2.1 in a heterologous expression system, suppressing K_V2.1 current density without changing kinetic parameters (18).

Despite the association of genetic variation in *KCNE5* with disease, knowledge regarding the underlying molecular mechanisms is sparse. Therefore, for the present study, we generated Kcne5 knockout ($Kcne5^{-/0}$) mice to determine the implications for cardiac function. Moreover, we examined how human *KCNE5* mutations that are linked to AF and BrS affect the K_V2.1 current.

MATERIALS AND METHODS

Kcne5 knockout mice

Kcne5 knockout mice were generated by the commercial provider Taconic (Oxnard, CA, USA) from a cryopreserved *Kcne5* knockout line (Taconic TF0342, background: 129/SvEv-C57BL/6) in their knockout repository. In these mice, the *Kcne5* gene is completely deleted. Positive clones were screened by Southern blot for correct targeting events. Genotyping was performed by PCR with primers 18 (5′-TGTATGCTTCATTCAGGGCC-3′) and 27 (5′-GGGTTC-AAATGATCTTCCTGCC-3′) to yield products of 313 bp for wild-type (WT) or 376 bp for mutant animals. Mice were bred and genotyped at Taconic and delivered to our university facilities at least 2 wk before the experiments. The mice were provided food and water *ad libitum* and housed in a room kept at 22°C with a 12-h light-dark schedule. Knockout (hemizygous, $Kcne5^{-/0}$) male mice were bred from WT ($Kcne5^{+/0}$) or hemizygous males ($Kcne5^{-/0}$) with heterozygous ($Kcne5^{-/+}$) female mice. $Kcne5^{-/0}$ mice are viable and fertile. We also generated a second $Kcne5^{-/0}$ mouse line, on a C57BL/6NCrl background, in collaboration with Dr. Boris Jerchow [Transgenic Core Facility, Max Delbrück Center for Molecular Medicine (MDC), Berlin, Germany], using a zinc finger approach (Supplemental Fig. S1). To verify the successful homology-directed repair in founder animals, we used PCR and enzyme digestion, as well as sequencing. Specific primers (Supplemental Fig. S1*A*, yellow and blue) were used for PCR analysis of genomic DNA. Positive founder animals, the DNA of which contained the new restriction site, displayed 2 fragments instead of 1 (Supplemental Fig. S1*B*). In addition, the positive founder animals were examined by sequencing (Supplemental Fig. S1*C*, primers yellow and gray). Sequence analysis showed correct homology-directed repair with the 3 stop codons (Supplemental Fig. S1*C*, underlined red) and the new *Tfi*I restriction site (underlined green) in the investigated animal. The breeding strategy for the generation and maintenance of $Kcne5^{-/0}$ mice was as follows: $y^{/+}$ (male) $x^{-/+}$ (female) to receive male $y^{/-}$ ($Kcne5^{-/0}$ mice) and $y^{/+}$ (*Kcne5* WT littermates). Genotyping was performed by PCR (Supplemental Fig. S1*D*). Neither $Kcne5^{-/0}$ mouse line exhibited cardiac hypertrophy, other overt structural defects, or $K_V\alpha$ subunit transcript remodeling; each exhibited similar ventricular myocyte K_V current upregulation. We conclude that the functional effects we observed in this study are specific to *Kcne5* deletion, as they arose in 2 different strains generated by different methodologies.

All animal work conformed to national guidelines for the protection of vertebrate animals used for experimental and other scientific purposes. All mice were housed in pathogen-free facilities, and experiments were approved by the Institutional Animal Care and Use Committees at University of California, Irvine, and at MDC-Berlin. Studies were performed during the light cycle, in strict accordance with the recommendations in the *Guide for the Care and Use of Laboratory Animals* of the National Institutes of Health (NIH), Bethesda, MD, USA. For all experiments requiring postmortem harvest of $Kcne5^{-/0}$ mouse tissue, each mouse was euthanized by CO_2 inhalation before cervical dislocation.

Heart size analysis

To compare the size of the hearts of adult (8-mo-old) male $Kcne5^{-/0}$ mice with age-matched control (WT), the mice were euthanized with CO_2 before cervical dislocation. After opening of the chest cavities, their hearts were transected below the major vessels and rinsed free of blood in normal saline. The saline was removed from the hearts with a napkin before being weighed. Furthermore, we isolated the right tibia, which was rinsed to remove skin and muscle tissue and measured from the crest to the medial malleolus. The size of the hearts was normalized to the length of the tibia and reported as the ratio of heart size (mg)/tibia length (mm). The unpaired Student's *t* test with Welch's correction was performed with Prism (GraphPad Software, La Jolla, CA, USA) for statistical analysis. Values of $P < 0.05$ were considered statistically significant. Data are expressed as means ± SEM.

Body surface electrocardiograph recordings

Mice were anesthetized with 2% isoflurane in oxygen and were spontaneously breathing. They were placed on a heating pad to avoid a dramatic drop in body temperature, while the subcutaneous needle electrodes on shield cables were placed on the left side near the middle part of the rib cage (plus electrode), in the right foreleg pit (minus electrode), and in the right hind leg (reference electrode), to record a single-lead surface ECG. Before signals were recorded, the isoflurane in the oxygen was lowered to 1.75%, and the heating pad was disconnected because of an increase in electrical noise. Signals were recorded for 5 min with Powerlab 8/35 (ADInstruments, Dunedin, New Zealand) at 2 kHz and filtered with a high-pass setting of 0.3 Hz and a low-pass setting of 1 kHz. Beats within min 1 and 4 of the recording were used to generate a mean-signal ECG and were analyzed manually with LabChart 7 (ADinstruments). The isoelectric level was calculated by the program from the pre-P wave segment or from the interval between the end of the P-wave and the beginning of the Q-wave, if possible. Because of electrical noise, the end of the T-wave was difficult to determine on the mean signal. Hence, the QT interval could not be determined accurately. Therefore, for each ECG recording, the mean QT interval was manually determined from 5 single heart beats showing a minimum of electrical noise. Unpaired Student's *t* test with Welch's correction was performed with Prism 5.01 for statistical analysis and values of $P < 0.05$ were considered statistically significant. Pooled data are expressed as means ± SEM.

Invasive electrophysiology studies

For invasive electrophysiology studies, we used a digital electrophysiology lab (EP Tracer; CardioTek, Maastricht, The Netherlands) and octapolar 2-French electrode catheters (CIBermouse Cath; Numed, Cross Roads, TX, USA), to determine standard parameters of electrical conduction and refractoriness and to test for inducibility of arrhythmias. Mice were lightly anesthetized with isoflurane (1.6 vol. % isoflurane/air) at a constant body temperature. The catheter was placed *via* the right jugular vein into the right atrium and ventricle. We performed programmed electrical stimulation with a standardized protocol with documentation of occurrence and duration of induced arrhythmias (19).

RNA extraction and reverse transcription

For expression analysis, mouse atria and the walls of each ventricle were isolated without excising the whole heart, frozen in liquid nitrogen, and kept at −80°C until further use. RNA was extracted from the atria and ventricles of male *Kcne5*$^{-/0}$ and control (*Kcne5*$^{+/0}$) mice by using the RNeasy RNA Purification Kit (Qiagen, Germantown, MD, USA), according to the manufacturer's protocol. The RNA was reverse-transcribed with the QuantiTect Reverse Transcription Kit (Qiagen) according to the manufacturer's instructions.

Human cardiac tissue samples from donor hearts that were unsuitable for transplantation were kindly provided by Dr. András Varró (University of Szeged, Szeged, Hungary). The procedure was approved by the national ethics committee, ethics approval number 4991-0/2010-1018EKU (339/PI/010), and informed consent was given to use the tissue for research purposes. The investigation conformed to the principles outlined in the Declaration of Helsinki. All donors received 25,000 Na-heparin, flushing solution (Custodiol; Dr. Franz Köhler Chemie, Bensheim, Germany), methylprednisolone sodium succinate (Solu-Medrol; Pfizer, New York, NY, USA), norephnephrine (Arterenol; MilliporeSigma, Burlington, MA, USA), and hydroxyethyl starch (Voluven; Pfizer) before heart explantation. The hearts were placed in ice-cold cardioplegic solution, cut into pieces, frozen, and stored in liquid nitrogen until further use. RNA extraction and cDNA generation from human heart tissues were performed as described by Soltysinska *et al*. (20).

Quantitative PCR

Quantitative analyses of the *KCNE5/Kcne5* gene in the cDNA samples from human and mouse hearts were performed in duplicate reactions of 20 μl volumes containing 10 μl PrimerDesign 2X Precision Mastermix (Primerdesign, Southampton, United Kingdom) with the 7300 qPCR System (Thermo Fisher Scientific, Waltham, MA, USA) and the CFX96 Real-Time PCR System (Bio-Rad, Hercules, CA, USA), respectively. Data were obtained with SDS1.2 software and CFX96 software, respectively. Double-dye assays were designed and synthesized by Primerdesign (primer sequences for mouse, sense: 5′-GCACGAAGAGACCTCAGACAT-3′, antisense: 5′-GGACAGGAAAACAAGAACACCAT-3′; and for human, sense: 5′-TACTTCCAAATGCCTCTCCTCTAT-3′, antisense: 5′-AACAACCTTTATTACCTGCCTCTG-3′). The amplification protocol used for each reaction was as follows: a 10 min initiation step at 95°C before 40 cycles of 15 s at 95°C and 1 min at 60°C. For optimal normalization analysis of the cDNA samples, we used the geNorm Reference Gene Selection Kit (Primerdesign) (21). β-Actin (*ACTB*) and topoisomerase-1 (*TOP1*) were chosen as optimal reference genes for the human cDNA samples, and for mouse cDNA samples, glyceraldehyde phosphate dehydrogenase, and *ActB* were used (Primerdesign). The $2^{-\Delta Ct}$ method (22) was used to determine the relative expression of *KCNE5/Kcne5* in both human and mouse cDNA samples. A 2-way ANOVA with Bonferroni *posthoc* and an unpaired Student's *t* test with Welch's correction were performed with using Prism 5.01 (GraphPad) for statistical analysis. Values of $P < 0.05$ were considered statistically significant. Data are expressed as means ± SEM.

Plasmids

Human K_V2.1 (GenBank Accession number NM_004975) in the eGFP-N1 vector (Takara Bio USA, Mountain View, CA, USA) and human KCNE5 (hKCNE5, NM_012282) in pXOOM are described in refs. 18 and 20. Mutant constructs P33S (c.97C > T), L65F (c.193C > T), R85H (c.254G > A), Y81H (c.241T > C) or D92E/E93X (c.276-277CG > AT) were generated by mutated oligo extension PCR with hKCNE5 in pXOOM as template using PfuUltraII HS Fusion Polymerase (Agilent Technologies, Santa Clara, CA, USA) and subsequent restriction with *Dpn*I (Thermo Fisher Scientific). Reaction samples were transformed into *Escherichia coli* XL1 Blue cells applying a standard heat-shock procedure. After plasmid DNA preparation, constructs were verified by complete DNA sequencing of the cDNA insert (Macrogen, Seoul, South Korea).

Ventricular tissue immunofluorescence

Cryosections (8 mm) from snap-frozen ventricular tissue were fixed with ice-cold acetone for 10 min at 4°C, blocked, and permeabilized in 10% goat serum, 0.3% Triton X-100 and 0.2% bovine serum albumin for 30 min. The following primary antibodies were used and incubated overnight at 4°C: rabbit anti-Kcne5 (1:20; MilliporeSigma, Burlington, MA, USA),

mouse anti-β-catenin (1:20; MilliporeSigma), rabbit anti-$K_V2.1$ (1:20; Thermo Fisher Scientific), and mouse anti-Cx43 (1:20; Thermo Fisher Scientific). As secondary antibodies we used AlexaFluor 555 goat anti-rabbit and AlexaFluor 647 goat anti-mouse (1:1000; Thermo Fisher Scientific), incubated for 60 min at room temperature. Kcne5 staining was amplified with biotin-conjugated anti-rabbit (1:500; Jackson ImmunoResearch Laboratories, West Grove, PA, USA) for 30 min followed by incubation with streptavidin-conjugated AlexaFluor 555 (1:1000; Thermo Fisher Scientific) for 60 min at room temperature. Stained cryosections were mounted with fluorescence mounting medium (Agilent Technologies) and imaged on a confocal laser scanning microscope (TSC SP5 with software, ver. LAS AF 2.632; Leica Microsystems, Wetzlar, Germany). Images were assembled in Photoshop CS4 (Adobe, San Diego, CA, USA) and CorelDraw 34 (Corel, Ottawa, ON, Canada).

Electrophysiological analysis of adult mouse cardiomyocytes

Ventricular cardiomyocytes were isolated from 7-mo-old male mice, as described in detail by Hu *et al*. (23). Only rod-shaped, quiescent cardiomyocytes with clear striations were used for recording. Whole-cell patch-clamp recordings from dispersed ventricular myocytes (derived from 2 to 8 mice of each genotype) were obtained at room temperature with an IX50 inverted microscope (Olympus, Center Valley, PA, USA) equipped with an FHD chamber from IonOptix (Westwood MA, USA) and a Multiclamp 700A Amplifier, a Digidata 1300 Analog/Digital converter, and a PC with pClamp9.2 software (all from Molecular Devices, Sunnyvale, CA, USA). For whole-cell patch-clamp recordings, the bath solution contained (in mM) 117 NaCl, 4 KCl, 1.7 $MgCl_2$, 10 4-(2-hydroxyethyl)-1-piperazineethanesulfonic acid, 1 KH_2PO_4, 4 $NaHCO_3$, 3 $CoCl_2$, and 10 D-glucose (pH 7.4 with NaOH). Bath solutions were treated with either no drug, 50 μM 4-aminopyridine (4-AP; ICN Biomedicals, Irvine, CA, USA), 25 mM tetraethylammonium (TEA; MilliporeSigma), or 500 nM heteropodatoxin (HpTx2) for K_V current inhibition. Pipettes were of 2.0–3.1 MΩ resistance when filled with intracellular solution containing (in millimolars) 130 KCl, 2 $MgCl_2$, 20 4-(2-hydroxyethyl)-1-piperazineethanesulfonic acid, 11 EGTA, 5 Na_2ATP, 0.4 Na_2GTP, and 5 Na_2CP (pH 7.4 with KOH). Outward K^+ currents were evoked during 4-s voltage steps to test potentials between −60 and +60 mV in 20 mV increments from a holding potential of −70 mV after a 100-ms prepulse to −40 mV. Uncorrected leak currents were always <100 pA. Data were analyzed with pClamp9.2 software (Molecular Devices), and statistical analysis (ANOVA) was performed with Origin 6.1 (Microcal, Northampton, MA, USA).

Human embryonic kidney cell culture, transient transfection, and patch-clamp electrophysiology

Human embryonic kidney (HEK)293 cells were cultured as previously described (18). HEK293 cell cultures (70–80% confluence) were cotransfected with 250 ng $K_V2.1$ and 1 μg WT or mutant hKCNE5 with Lipofectamine 2000 reagent (Thermo Fisher Scientific). Green fluorescent protein cDNA (0.5 μg) was cotransfected as a transfection marker. Transfected cells were dissociated with trypsin and used for electrophysiological analysis 16–24 h after transfection. Patch-clamp recordings from HEK293 cells were performed as previously described (18). Series resistance was compensated (80%) for, and cells with a voltage error exceeding 5 mV after compensation were excluded from analysis. The Boltzmann equation, $y = 1/\{1+\exp[-(V-V_{1/2})/k]\}$, where V is the voltage applied, $V_{1/2}$ is the voltage at which 50% of the channels are (in)activated, and k is the slope factor, was used to fit the voltage-dependence of activation and inactivation. Single and double exponential functions were used to fit the activation and deactivation kinetics, respectively. Student's t test or Mann-Whitney rank sum test was used for statistical analysis, and values of $P < 0.05$ were considered statistically significant.

HL-1 cell culture, transient transfection, and imaging

HL-1 cells were cultured and transfected in gelatin/fibronectin-coated T25 flasks (Nunc, Roskilde, Denmark) with Claycomb medium (MilliporeSigma), supplemented with 10% fetal bovine serum (Batch 11A568; MilliporeSigma), 100 U/ml penicillin (Thermo Fisher Scientific), 100 mg/ml streptomycin (Thermo Fisher Scientific), 0.1 mM norepinephrine (MilliporeSigma), and 2 mM L-glutamine (MilliporeSigma) at 37°C in 5% CO_2. At 90–100% confluence, the cells were trypsinized and resuspended in 5 ml medium, and 1.25 ml cell solution was transfected with 2 μg DNA in total, with 3.5 μl Silentfect Lipid Reagent (Bio-Rad) according to the manufacturer's protocol. Transfected cells were plated into a 35-mm tissue culture dish (Greiner Bio-One, Frickenhausen, Germany) containing 4 glass cover slips (diameter, 12 mm; Thermo Fisher Scientific) and coated with gelatin/fibronectin. The cells were incubated at 37°C in 5% CO_2 for 16–24 h before they were fixed by adding 4% paraformaldehyde in PBS for 10 min at room temperature.

Immunofluorescence staining and imaging with the LSM710 or LSM780 laser scanning confocal microscope (Zeiss, Jena, Germany) were performed with published methods (18, 24). Primary antibodies were: rabbit polyclonal anti-KCNE5 (1:100, in-house) (18), mouse monoclonal anti-$K_V2.1$ (1:100, clone K39/25; NeuroMab, University of California, Davis/NIH NeuroMab Facility, Davis, CA, USA), and rat monoclonal anti-hemagglutinin (HA) (1:50, clone 3F10; Roche Diagnostics, Indianapolis, IN, USA). Alexa-Fluor 647–conjugated and rhodamine-conjugated phalloidin (1.5 U/ml; Thermo Fisher Scientific) were used as plasma membrane markers in HL-1 cells. Rat monoclonal anti-lysosomal-associated membrane protein (LAMP)-2 (1:100, clone GL2A7; Abcam, Cambridge, United Kingdom) was used as a lysosomal marker. Depending on the antibodies used, the plasma membrane was visualized with either rhodamine-conjugated phalloidin or Alexa Fluor 647 phalloidin to identify the submembranous F-actin in HL-1 cell secondary antibodies: AlexaFluor 488 donkey anti-rabbit IgG [heavy (H)+light (L) chain] (1:200), AlexaFluor 488 donkey anti-mouse IgG (H+L) (1:200), AlexaFluor 488 donkey anti-rat (H+L) (1:200), AlexaFluor 568 donkey anti-rabbit IgG (H+L) (1:500), and AlexaFluor 555 donkey anti-mouse IgG (H+L) (1:500). All secondary antibodies were purchased from Thermo Fisher Scientific.

RESULTS

The *KCNE5* gene is expressed in both mouse and human hearts

In WT ($Kcne5^{+/0}$) male mice, we detected *Kcne5* transcript in both the atria and ventricles (**Fig. 1*A***). Because the level of KCNE5 expression in the human heart is still a matter of debate (5–7), we also analyzed the relative expression in cardiac tissue samples from 6 male donor

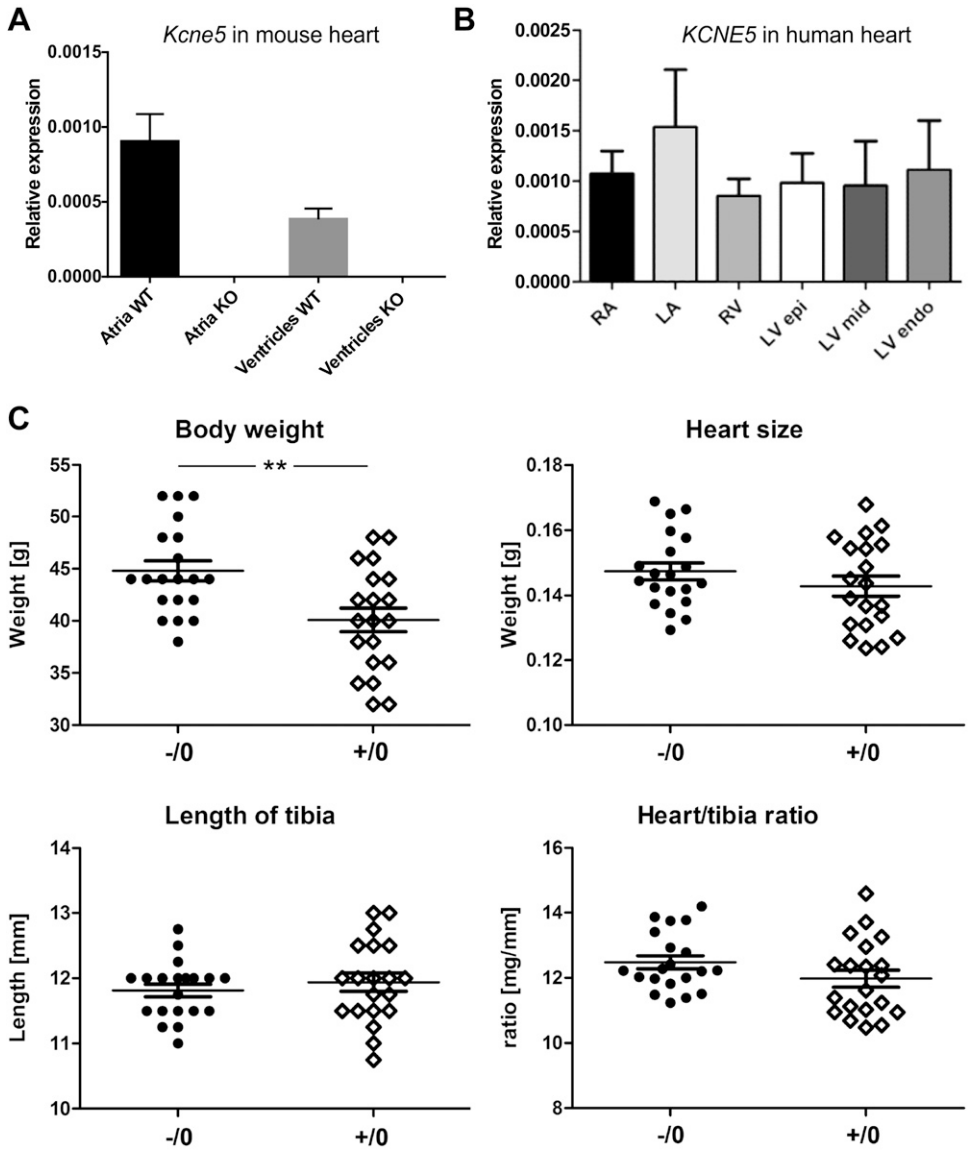

Figure 1. *Kcne5* is expressed in mouse and human hearts. *A*) Quantification of *Kcne5* transcript expression in atria and ventricles (n = 5 and n = 6, respectively) for male $Kcne5^{+/0}$ (WT) and $Kcne5^{-/0}$ (knockout) mice by real-time qPCR, normalized to the reference genes *ActB* and glyceraldehyde phosphate dehydrogenase. Data are means ± SEM. *B*) Relative *KCNE5* regional expression in male human hearts (n = 6): left (LA) and right (RA) atria and the left ventricular epi-, mid- and endomyocardial wall. No significant differences in expression levels between the regions were found. Quantification was by real-time qPCR with *ACTB* and *TOP1* as reference genes. *C*) Body weight, heart size, and tibia length of ~8-mo-old male mice (n = 20 in each group; means ± SEM shown). $Kcne5^{-/0}$ mice showed a significant increase in body weight (44.8 ± 1.0 g) compared to control mice (40.1 ± 1.1 g). P = 0.0030. Heart size (0.147 ± 0.003 *vs.* 0.143 ± 0.003 g, respectively) and the length of tibia (11.8 ± 0.1 *vs.* 11.9 ± 0.1 mm, respectively) did not show any differences. Likewise, there was no difference in heart size when normalized to tibia length [(mg/mm) 12.5 ± 0.2 *vs.* 12.0 ± 0.3, respectively]. $^{**}P < 0.01$.

hearts, and found that the *KCNE5* gene was expressed in all human heart regions analyzed (Fig. 1*B*).

Kcne5 deletion predisposes to ventricular arrhythmia

Because we found that $Kcne2^{-/-}$ pups from homozygous crosses show cardiac hypertrophy as early as 3 wk (25), we investigated whether deletion of *Kcne5* had a similar effect (Fig. 1*C*). *Kcne5* deletion did not alter heart weight, normalized to either body weight or tibia length, in either of the strains we assessed (Fig. 1*C* and Supplemental Table S1). In addition, echocardiographic analysis uncovered no evidence of cardiac hypertrophy (Supplemental Table S2).

Noninvasive body surface ECG analysis in anesthetized male mice (Supplemental Fig. S2), aged ~5 mo (n = 9–10 in each group) (Supplemental Fig. S2*A*) and 8 mo (n = 16–20 in each group) (Supplemental Fig. S2*B*), did not reveal any genotype-dependent changes. In contrast, invasive ECG uncovered ventricular premature beats (VPBs), which were followed by postextrasystolic compensatory pauses, in male $Kcne5^{-/0}$ mice (**Fig. 2*A***). In 1 $Kcne5^{-/0}$ mouse, we observed a spontaneously occurring episode of polymorphic ventricular tachycardia VT. The episode could not be terminated by burst pacing, but eventually converted into an atrial arrhythmia with a 2:1 and 3:1 atrioventricular conduction, (Fig. 2*B*). The $Kcne5^{-/0}$ mice also had increased susceptibility to polymorphic VT induction with a defined pacing protocol followed by 3 extra stimuli (Fig. 2*C, D*). Furthermore, *Kcne5* deletion shortened the ventricular effective refractory period (Fig. 2*E*).

Kcne5 gene deletion augments specific ventricular K_V currents

We next used whole-cell patch-clamp electrophysiology to quantify K_V currents in ventricular myocytes from adult

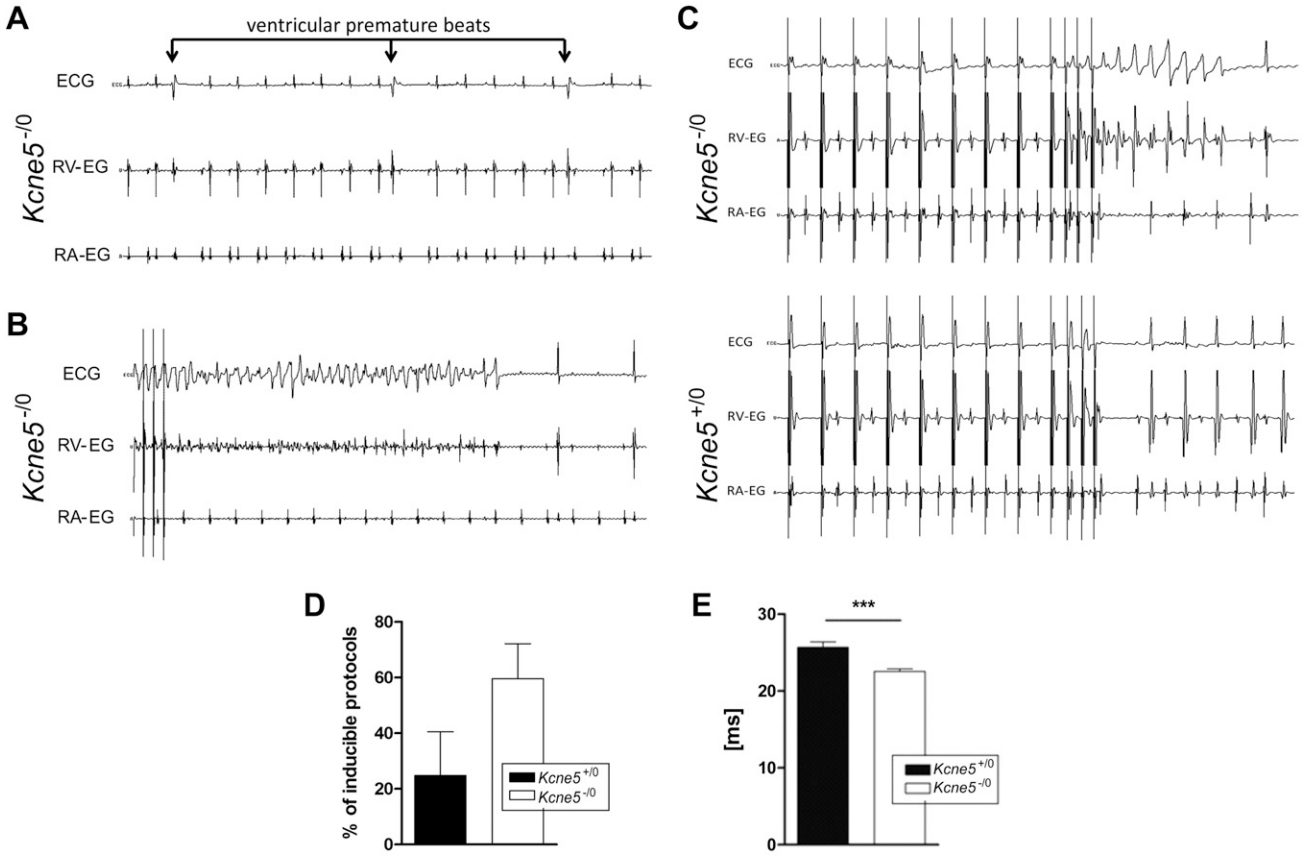

Figure 2. *Kcne5* deletion causes ventricular arrhythmias. *A*) Spontaneously occurring monomorphic VPBs were detectable during continuous ECG monitoring in sedated live $Kcne5^{-/0}$ mice. No such VPBs were found in $Kcne5^{+/0}$ mice. Upper ECG curves represent body surface ECGs, middle ECG curves represent intracardiac ECG from the ventricular catheter, and lower ECG curves represent intracardiac ECG registration from the atrial catheter. Note postextrasystolic compensatory pauses after VPBs are pathognomonic for ventricular extrasystolic beats. *B*) A spontaneously occurring episode of polymorphic VT was noted in 1 $Kcne5^{-/0}$ mouse. The episode could not be terminated by burst pacing (pacing spikes on the left). The VT finally converted into an atrial arrhythmia with a 2:1 and 3:1 atrioventricular conduction. *C*) Polymorphic VTs were inducible during continuous ECG monitoring of sedated live $Kcne5^{-/0}$ mice. After a defined pacing protocol followed by 3 extrastimuli polymorphic VTs were highly inducible in $Kcne5^{-/0}$ mice as compared to WT controls. Data for ECG curves were obtained as described in *A*. *D*) Percentage of inducible protocols was increased in $Kcne5^{-/0}$ mice *vs.* WT controls. *E*) The ventricular effective refractory period was reduced in $Kcne5^{-/0}$ mice *vs.* $Kcne5^{+/0}$ controls. $^{***}P < 0.001$.

male mice, to examine possible mechanisms for arrhythmogenesis in $Kcne5^{-/0}$ mice. In previous studies of adult mice, it was discovered that their ventricular myocyte K_V current is composed primarily of the fast outward transient current ($I_{to,f}$), which is generated by $K_V4.2$, $K_V4.3$, or both channels and is sensitive to heteropodotoxin (HpTx)-2; the slow transient outward current ($I_{to,s}$), probably generated by $K_V1.4$ ($I_{K,slow}$); and a steady-state component (I_{ss}) (26). $I_{K,slow}$ comprises the 50 μM 4-AP-sensitive $K_V1.5$ current ($I_{K,slow1}$) (27, 28) and the 25 mM TEA-sensitive $K_V2.1$ current ($I_{K,slow2}$) (27, 29). We studied ventricular myocytes isolated from the apex (**Fig. 3**) and the septum (**Fig. 4**). Similar to our prior work with the $Kcne2^{-/-}$ mouse line (30), we found that apical myocytes isolated from either $Kcne5^{-/0}$ or $Kcne5^{+/0}$ mice lacked $I_{to,s}$, whereas septal myocytes were divided roughly equally into those with $I_{to,f}$ and those without (as assessed by curve fitting the current decay at +40 mV) (**Table 1**).

In apical myocytes, *Kcne5* deletion increased peak total K_V current density by 22% (Fig. 3*A, B*). As assessed by curve fitting, the primary effect in apical myocytes of *Kcne5* deletion was a 36% increase in $I_{K,slow}$ density. *Kcne5* deletion also increased apical myocyte $I_{to,f}$ density, by 20% (Table 1). We next used pharmacological analysis as an additional methodology for quantifying effects on myocyte K_V currents. In apical myocytes, *Kcne5* deletion increased the density at +60 mV of both components of $I_{K,slow}$: the 50 μM 4-AP-sensitive $K_V1.5$ current ($I_{K,slow1}$) by 78% and the 25 mM TEA-sensitive $K_V2.1$ current ($I_{K,slow2}$) by 30%. The apical myocyte HpTx2-sensitive K_V4 current ($I_{to,f}$) was increased by 13% by *Kcne5* deletion, although the increase did not reach statistical significance (Fig. 3*C–H*). Thus, the results of curve fitting and pharmacological analyses were essentially congruent.

In the septum, *Kcne5* deletion increased the myocyte peak total K_V current density at +40 mV by 32% in

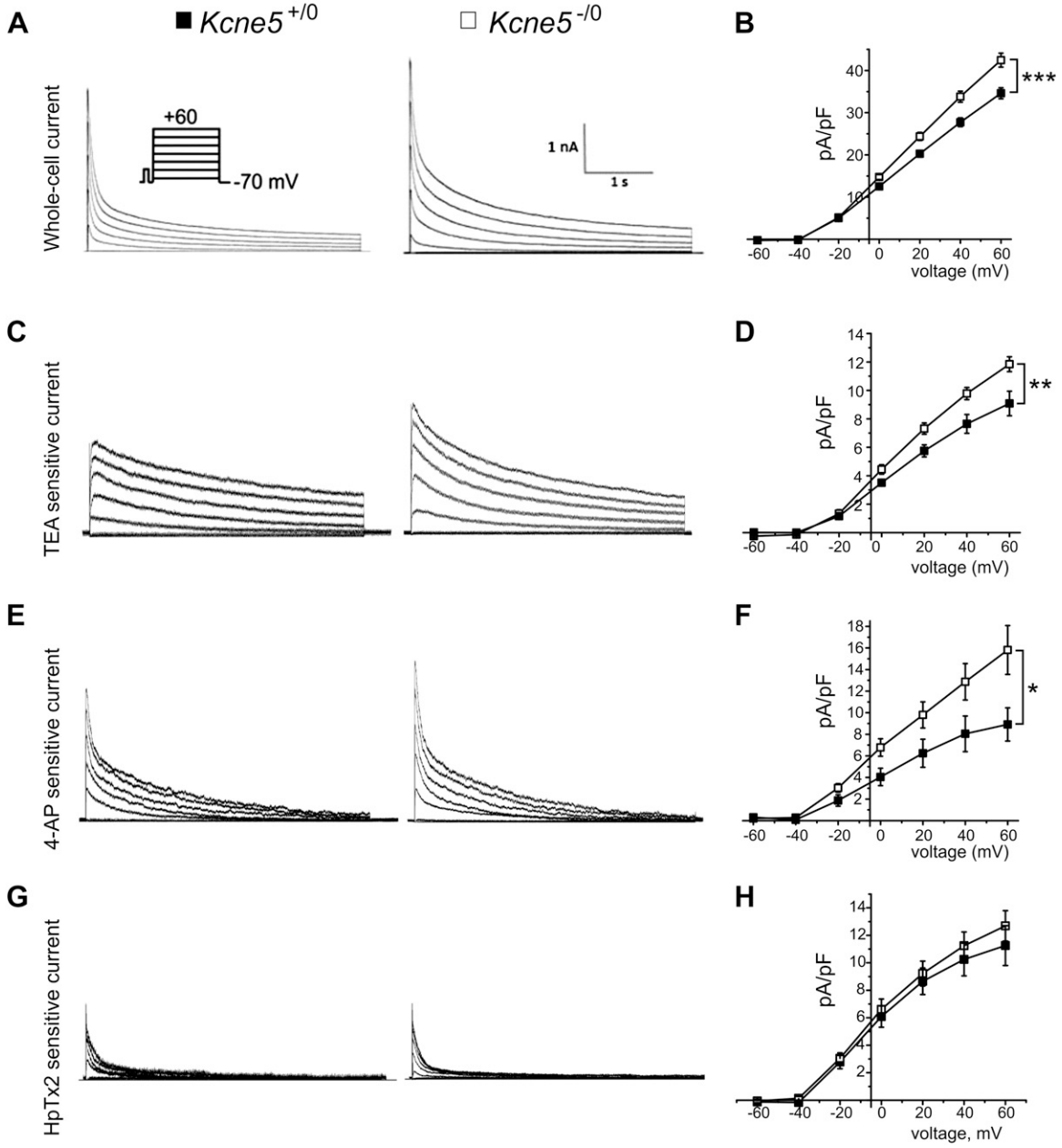

Figure 3. *Kcne5* gene deletion augments ventricular apical myocyte K_V currents. *A*) Representative native whole-cell K_V currents in *Kcne5*$^{+/0}$ (left) and *Kcne5*$^{-/0}$ (right) ventricular apex cardiomyocytes (voltage protocol inset) (n = 27–31). *B*) Mean current density *vs.* voltage characteristics (*I-V* curve) from recordings as in *A* for *Kcne5*$^{+/0}$ (filled squares) and *Kcne5*$^{-/0}$ (open squares) apical myocytes (n = 27–31). ***$P < 0.001$ at +60 mV. *C*) Typical digitally subtracted 25 mM TEA-sensitive current ($I_{K,slow2}$) for *Kcne5*$^{+/0}$ (left) and *Kcne5*$^{-/0}$ (right) ventricular myocytes. *D*) Mean *I-V* relationships for TEA-sensitive currents as in *C* (n = 9–10 cells/genotype, derived from 3 mice/genotype). **$P = 0.01$ at +60 mV. *E*) Typical digitally subtracted current traces for 50 μM 4-AP-sensitive current ($I_{K,slow1}$) for *Kcne5*$^{+/0}$ (left) and *Kcne5*$^{-/0}$ (right) ventricular myocytes. *F*) Mean *I-V* relationships for myocytes as in *E* (n = 9–10 cells/genotype, derived from 5 mice/genotype). $P < 0.05$ at +60 mV. *G*) Typical digitally subtracted 500 nM HpTx-sensitive current ($I_{K,slow2}$) for *Kcne5*$^{+/0}$ (left) and *Kcne5*$^{-/0}$ (right) ventricular myocytes. *H*) Mean *I-V* relationships for HpTx-sensitive currents as in *G* (n = 6 cells/genotype, derived from 4 to 5 mice per genotype). $P = 0.45$ at +60 mV.

myocytes lacking $I_{to,f}$, but left the peak total K_V current unchanged in septal myocytes with $I_{to,f}$ (Fig. 4*A, B*). As quantified by curve fitting, the sole effect of *Kcne5* deletion on specific currents in the septum was an increase in $I_{K,slow}$ density by 36% in septal myocytes lacking $I_{to,f}$. In contrast, *Kcne5* deletion left $I_{K,slow}$, $I_{to,s}$, and $I_{to,f}$ density unchanged in septal myocytes with $I_{to,f}$ (Table 1). Pharmacological analysis in a population of septal myocytes including both those with $I_{to,f}$ and those without (as assessed by curve fitting) showed that mean *Kcne5*$^{-/0}$ septum myocyte K_V2.1 (25 mM TEA-sensitive) current ($I_{K,slow2}$) amplitude was 37% greater at +40 mV than that of *Kcne5*$^{+/0}$ myocytes (Fig. 4*C, D*). In contrast, K_V1.5 (50 μM 4-AP-sensitive) current ($I_{K,slow1}$)

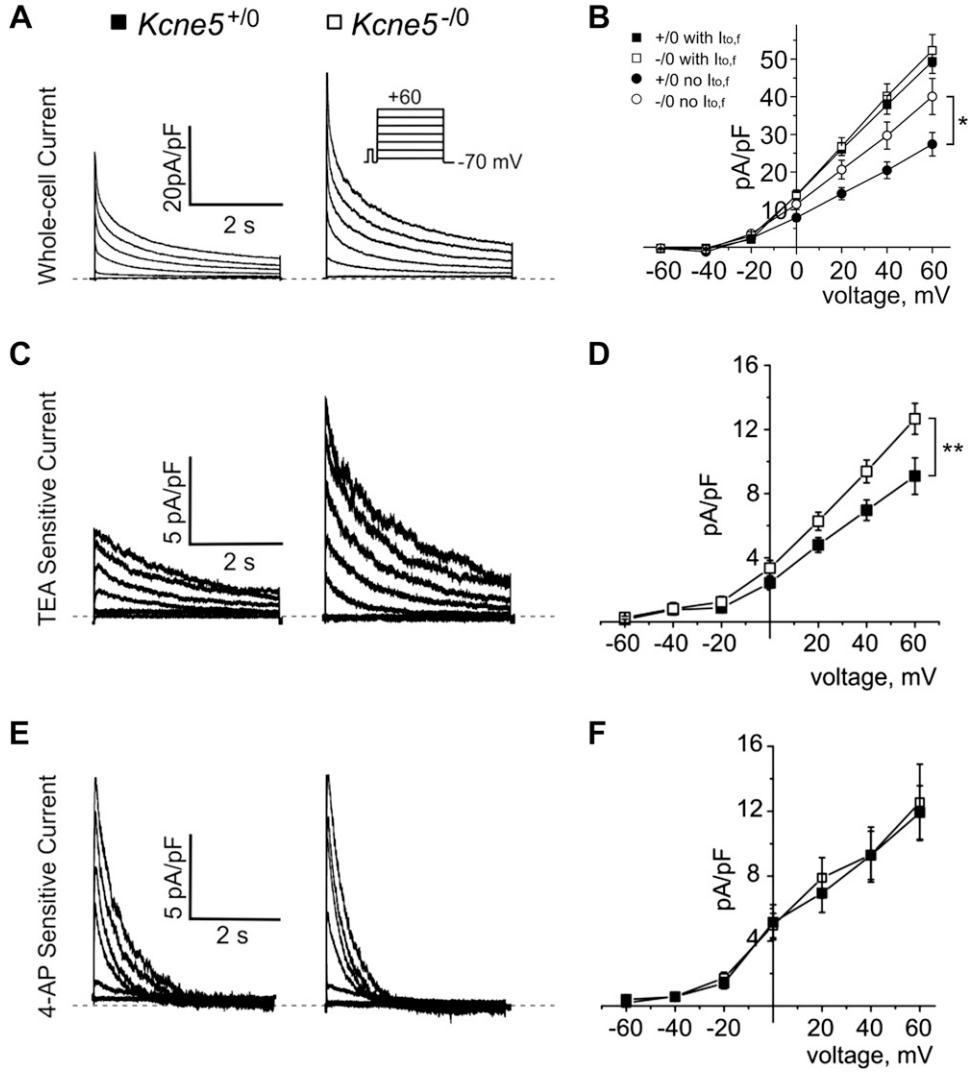

Figure 4. *Kcne5* gene deletion augments $I_{K,slow2}$ in ventricular septum myocytes lacking $I_{to,f}$. *A*) Typical current traces from $Kcne5^{+/0}$ and $Kcne5^{-/0}$ adult ventricular septum myocytes (voltage protocol inset). *B*) Mean *I-V* relationships for $Kcne5^{+/0}$ (solid) and $Kcne5^{-/0}$ (open) septal myocytes with (squares) or without (circles) $I_{to,f}$ ($n = 15$–19 cells per group). $^*P < 0.05$ at +60 mV. *C*) Typical digitally subtracted 25 mM TEA-sensitive $K_V2.1$ current ($I_{K,slow2}$) for $Kcne5^{+/0}$ (left) and $Kcne5^{-/0}$ (right) ventricular septum myocytes. *D*) Mean *I-V* relationships for TEA-sensitive currents as in *C* ($n = 6$ cells/genotype, derived from 2 mice/genotype). $^{**}P = 0.009$ at +60 mV. *E*) Typical digitally subtracted current traces for 50 μM 4-AP-sensitive $K_V1.5$ current ($I_{K,slow1}$) for $Kcne5^{+/0}$ (left) and $Kcne5^{-/0}$ (right) ventricular myocytes. Dashed lines: 0 current level. *F*) Mean I/V relationships for myocytes as in *E* ($n = 8$ cells/genotype, derived from 2 mice/genotype). $P = 0.984$ at +60 mV. Dashed lines: 0 current level.

amplitude at +40 mV was unchanged by *Kcne5* deletion (Fig. 4*E, F*). HpTx2 sensitivity was not quantified in septal myocytes because of the challenges of pharmacologically assessing $I_{to,f}$ with a toxin in this mixed cell population. As described above, curve-fitting data indicated that *Kcne5* deletion did not alter $I_{to,f}$ in the septum (Table 1). Finally, *Kcne5* deletion did not alter ventricular $K_V\alpha$ subunit transcript expression (Supplemental Fig. S3),

TABLE 1. *Fitted K_V current densities and inactivation kinetics in ventricular apex and septum myocytes from* $Kcne5^{+/0}$ *and* $Kcne5^{-/0}$ *mice at +40 mV*

Genotype and myocyte type	$I_{to,f}$	$I_{to,s}$	$I_{K,slow}$	n
$Kcne5^{+/0}$ apex	68.6 ± 2.5	NA	1351 ± 59.5	27
	14.7 ± 0.9	NA	8.5 ± 0.6	27
$Kcne5^{+/0}$ septum,	52.1 ± 3.3	526.3 ± 35	3869 ± 943	19
with $I_{to,f}$	14.3 ± 1.6	9.2 ± 0.5	11.2 ± 1.0	19
$Kcne5^{+/0}$ septum,	NA	165.7 ± 11.6	1601.8 ± 76	16
no $I_{to,f}$	NA	5.8 ± 0.8	9.5 ± 1.1	16
$Kcne5^{-/0}$ apex	66.7 ± 2.6	NA	1134 ± 31.4***	31
	17.5 ± 0.9*	NA	11.6 ± 0.7***	31
$Kcne5^{-/0}$ septum,	40.8 ± 1.8**	383.9 ± 22.8***	1857 ± 135	15
with $I_{to,f}$	16.3 ± 1.4	8.6 ± 1.1	11.2 ± 1.1	15
$Kcne5^{-/0}$ septum,	NA	159.2 ± 15	1250 ± 88***	16
no $I_{to,f}$	NA	8.5 ± 1.4	12.9 ± 1.7*	16

Values are means ± SE. Current properties: τ_{decay} (ms); I (pA/pF). I, current density; τ_{decay}, inactivation time constant; n, number of cells; NA, not applicable (current not present). Statistically significant changes in current density are underlined. $^*P < 0.05$, $^{**}P < 0.01$, $^{***}P < 0.005$ *vs.* equivalent criteria in WT mice.

suggesting that the effects on currents were primarily from loss of Kcne5 interaction rather than from transcript remodeling.

Kcne5 and K_V2.1 colocalize at ventricular myocyte intercalated discs

We analyzed the K_V2.1-Kcne5 interaction in more detail, because it occurred in both apical and septal myocytes. Using immunofluorescence, we found that Kcne5 localizes strongly to the intercalated discs (ICDs) in ventricular myocytes, with *Kcne5*$^{-/0}$ tissue serving as a negative control for antibody specificity (**Fig. 5*A***) and β-catenin as a marker for the ICDs (Fig. 5*B*). Similarly, we detected K_V2.1 strongly localized to the ICDs, using Connexin 43 as an ICD marker in these experiments (Fig. 5C). There was no evidence that *Kcne5* deletion altered the ability of K_V2.1 to specifically target the ICDs and no evidence of increased K_V2.1 protein expression overall.

K_V2.1 and KCNE5 colocalize at the plasma membrane and in intracellular vesicles in HL-1 cells

To facilitate more detailed analysis of KCNE5-K_V2.1 localization and examination of both mouse and human subunits, we used transient expression of epitope-tagged KCNE5 and K_V2.1 in the mouse atrial cardiomyocyte tumor lineage HL-1. When individually expressed, detection with an in-house KCNE5-specific antibody revealed that human KCNE5 was located both in small, dense clusters, and in some vesicle-like structures (**Fig. 6*A***). The ratio between these 2 different entities varied. To address possible species differences, we also transfected HL-1 cells with mouse *Kcne5*. The mouse protein localized similar to the human protein in these cells (Supplemental Fig. S4). To deduce whether these KCNE5$^+$ clusters were at the membrane or inside the cell, we generated an N-terminal, HA-tagged KCNE5 construct. The tag did not disturb the trafficking of the subunit, as the HA-KCNE5 localized similarly to the untagged KCNE5 (Fig. 6*B*), nor did the tag affect biophysical properties when coexpressed with K_V2.1 (Supplemental Fig. S5). When a specific HA-tag antibody was applied without permeabilizing the cell (Fig. 6*C*, surface), the same dense clusters appeared, indicating plasma membrane expression. Permeabilization of the same cells and exposure to the anti-KCNE5 antibody revealed additional KCNE5$^+$ intracellular vesicles (whole cell).

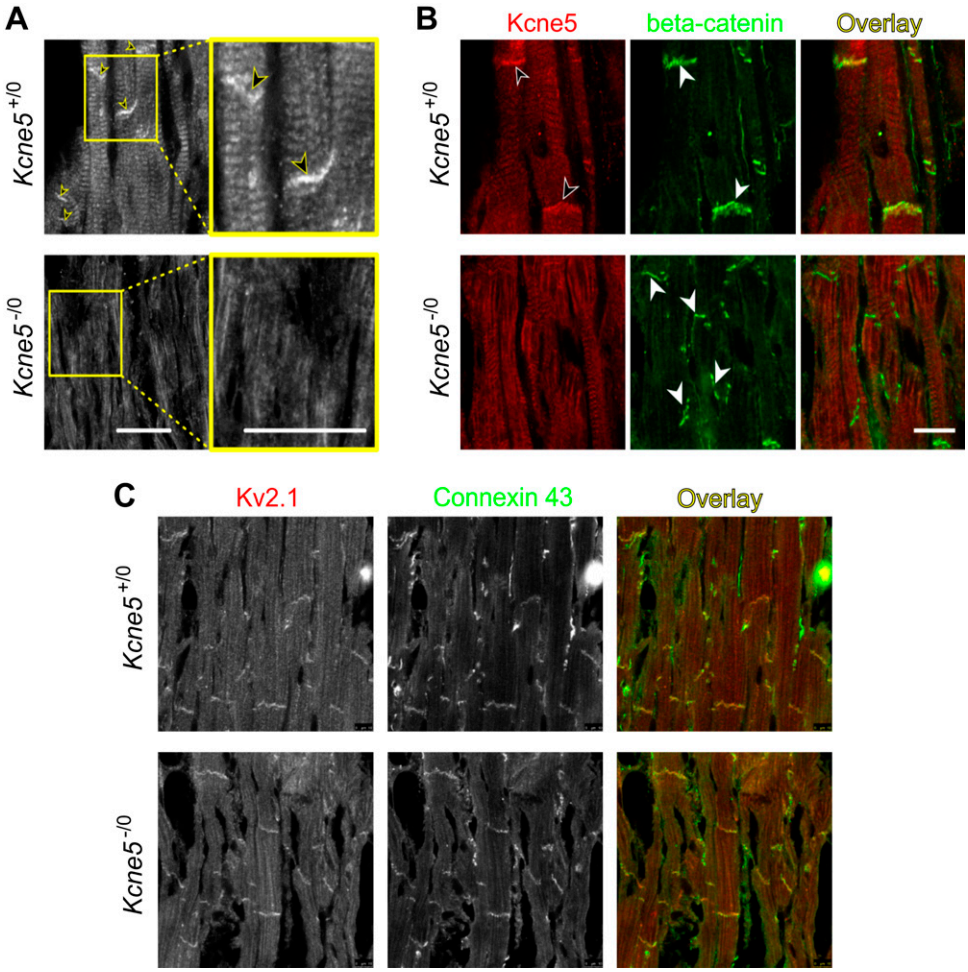

Figure 5. *K*cne5 and K_V2.1 colocalize in the ICD of mouse ventricular cardiomyocytes. *A*) Immunofluorescence staining of ventricular heart sections of *Kcne5*$^{+/+}$ and *Kcne5*$^{-/-}$ mice with an anti-Kcne5 antibody. *Kcne5* is detectable in ICDs of cardiomyocytes (arrows) whereas *Kcne5* signal is absent in *Kcne5*$^{-/-}$ hearts. Yellow framed areas are shown in higher magnification as indicated. *B*) Coimmunofluorescence staining with antibodies against *Kcne5* (red) and β-Catenin (green) for ICD visualization. No *Kcne5* signal was detectable in *Kcne5*$^{-/-}$ hearts. *C*) Coimmunofluorescence staining with antibodies against K_V2.1 (red) and Connexin-43 (green) as ICD marker proteins. Scale bars, 20 μm.

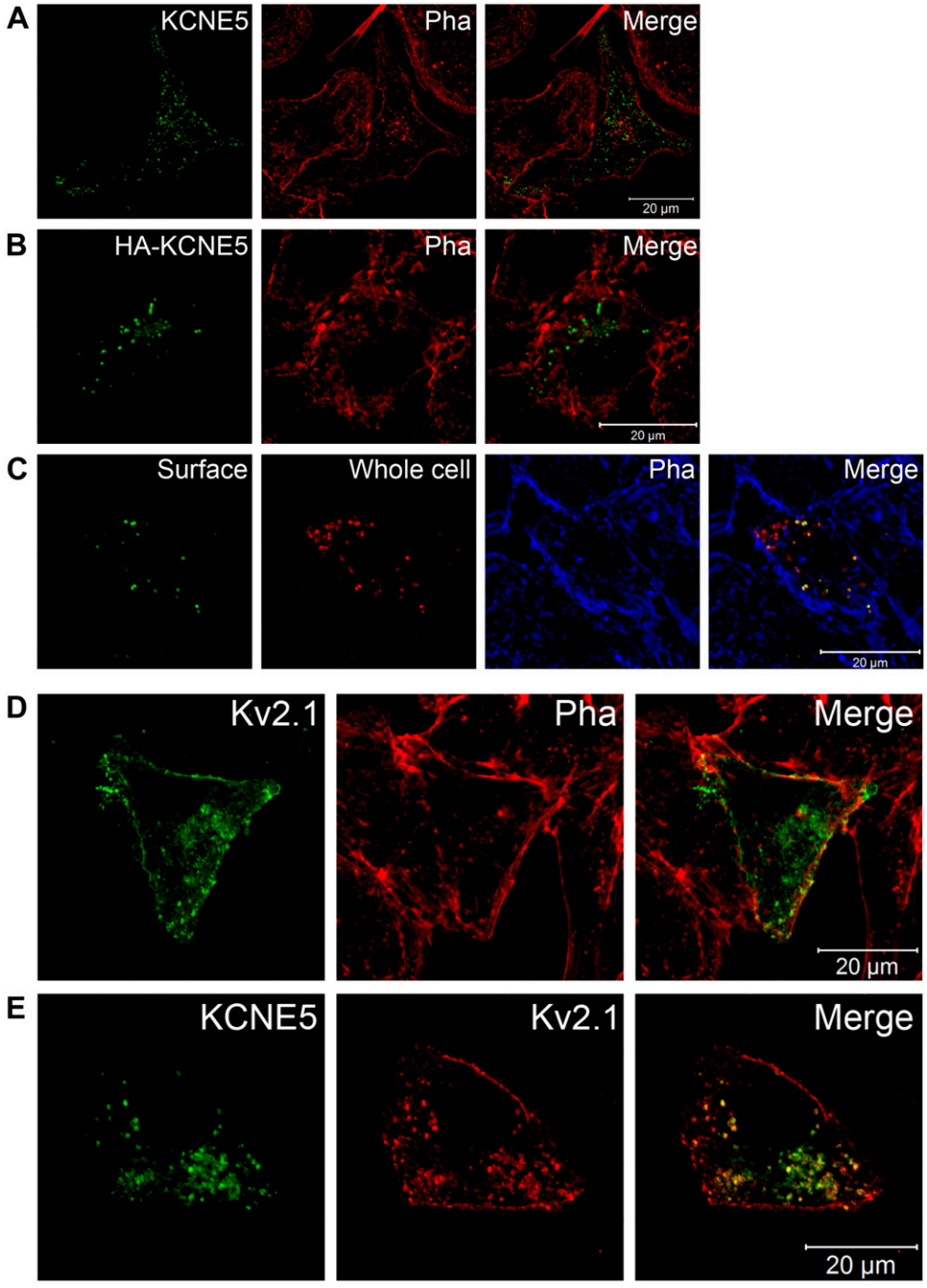

Figure 6. KCNE5 and $K_V2.1$ colocalize in HL-1 cells. *A*, *B*) Confocal images of HL-1 cells heterologously expressing WT KCNE5 (*A*) or HA-tagged WT KCNE5 (*B*). Phalloidin (Pha) labeled the submembranous actin cytoskeleton and was used to visualize the cell membrane. *C*) Nonpermeabilized HA-KCNE5–expressing HL-1 cells stained with a specific HA-tagged antibody (surface staining, green), permeabilized, and then stained with a KCNE5-specific antibody (red) and Phalloidin (blue). *D*) Colabeling of single transfected $K_V2.1$ (green) and endogenous Phalloidin (red) in HL-1 cells. *E*) Colabeling of cotransfected KCNE5 (green) and $K_V2.1$ (red) in HL-1 cells.

Next, we evaluated colocalization of KCNE5 with $K_V2.1$ in mouse atrial cardiomyocyte tumor lineage HL-1 cells. When expressed alone, $K_V2.1$ was predominantly located at the cell surface, overlapping phalloidin, which labels the actin cytoskeleton just beneath the plasma membrane. In most cells $K_V2.1$ could also be found in dense clusters and vesicles, similar to KCNE5 and consistent with results from studies of HEK293 cells (20, 30–33) (Fig. 6*D*). Upon coexpression of KCNE5 with $K_V2.1$, the channel subunits colocalized in the same clusters and vesicles in most of the cells (Fig. 6*E*), also in line with our recent results in HEK293 cells (18). Upon costaining with LAMP-2, we observed that KCNE5 and $K_V2.1$ localized to intracellular compartments that were in proximity to the lysosomes, indicative of late endosome compartments (**Fig. 7*A*–*C***).

Arrhythmia-associated KCNE5 mutations confer functional changes on the $K_V2.1$-KCNE5 channel complex

Although $K_V2.1$ is primarily characterized in rodent cardiac electrophysiology (31, 32), both $K_V2.1$ mRNA (33) and protein (34) are reportedly expressed in human atria and ventricles. With further evidence of

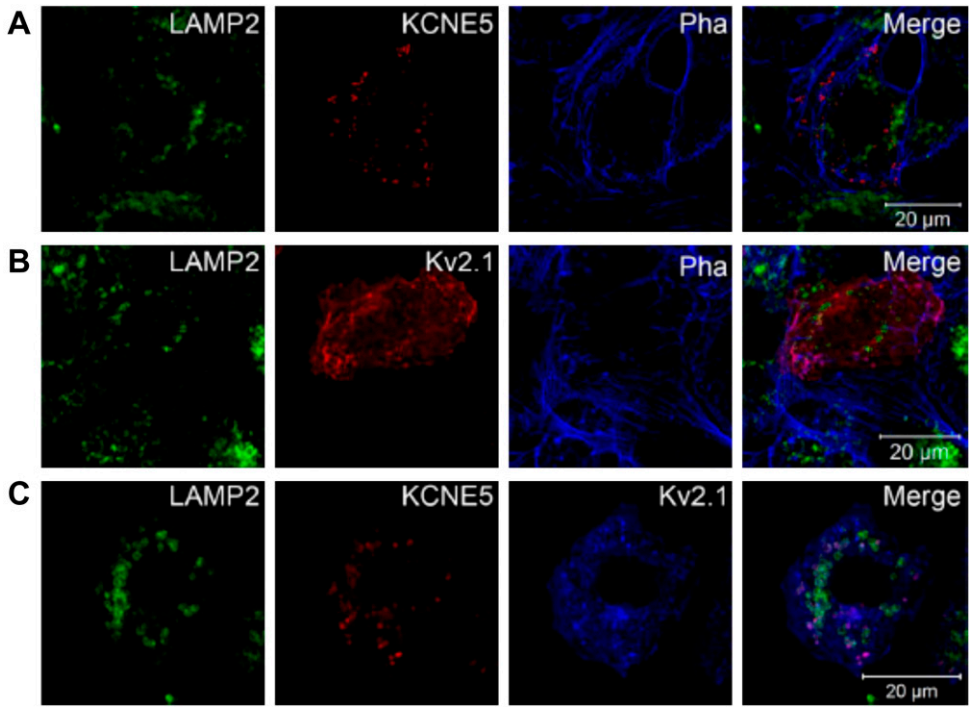

Figure 7. KCNE5 and $K_V2.1$ colocalize in intracellular compartments in proximity to the lysosomes. *A*, *B*) Laser confocal microscopy was used to acquire images of KCNE5 and $K_V2.1$ subunits singly transfected into HL-1 cells, respectively. Both were found to be located in dense clusters and vesicles for which some appear very close to the lysosomal marker LAMP2. Phalloidin (Pha) was used to identify the cell membrane. *C*) When $K_V2.1$ and KCNE5 were coexpressed in the same HL-1 cells, they colocalized in vesicles and dense clusters, similar to the above-mentioned structures, which again were located in proximity to the lysosome maker, LAMP2—possibly indicative of late endosome compartments.

an interaction between KCNE5 and $K_V2.1$ from our previous work (18) and the current study, we next investigated the effect of human KCNE5 genetic variants that had been linked to AF and BrS (15–17, 35). We coexpressed the KCNE5 AF variants P33S, L65F, or R85H (**Fig. 8**) and the KCNE5 BrS variants Y81H or D92E/E93X (**Fig. 9**) with $K_V2.1$ in HEK293 cells. Currents generated by $K_V2.1$ with KCNE5-P33S and Y81H were similar to those generated by $K_V2.1$ and WT KCNE5. In contrast, KCNE5-L65F shifted both the $K_V2.1$ voltage dependence of activation (Fig. 8*A*–*C*) and the voltage-dependence of inactivation (Fig. 8*D*) ~10 mV toward negative potentials. KCNE5-L65F also modified the $K_V2.1$ activation kinetics significantly (with a ~2-fold acceleration at 0 mV) without affecting the deactivation kinetics (Fig. 8*E*). In addition, KCNE5-L65F increased the $K_V2.1$ current density (~2-fold) compared with KCNE5-WT (243 ± 55 and 100 ± 25 pA/pF, respectively) (Fig. 8*F*). Coexpression of $K_V2.1$ with KCNE5-R85H changed neither the voltage-dependence of inactivation (Fig. 8*D*) nor the activation or deactivation kinetics (Fig. 8*E*). Yet, KCNE5-R85H tended to shift the voltage dependence of activation toward positive potentials (Fig. 8*C*) and to further reduce $K_V2.1$ current density (Fig. 8*F*), albeit not reaching statistical significance. KCNE5-D92E/E93X shifted the $K_V2.1$ voltage-dependence of activation (Fig. 9*A*–*C*) ~6 mV toward more negative potentials. Data for channels containing mutant KCNE5 are summarized in **Table 2**. The mutant forms of KCNE5 did not perturb KCNE5 trafficking in mouse atrial cardiomyocyte tumor lineage HL-1 cells (36) (**Fig. 10*A*–*C***). Thus, the KCNE5-L65F and D92E/E93X mutations exerted their effects by their impact on the electrical properties of $K_V2.1$.

DISCUSSION

Human KCNE5 sequence variants are associated with both AF (16, 17) and BrS (15), conditions that increase the risk of mortality (35, 36). The functional mechanisms linking KCNE5 to these cardiac arrhythmia syndromes have been suggested to be dysregulation of I_{Kslow} (16) or I_{to} (15), respectively, but little is known of the roles of KCNE5 *in vivo*. To aid in this endeavor, we studied the effects of germline deletion of *Kcne5* in mice. Transgenic mouse models have been instrumental in detecting and characterizing novel native functions of KCNE subunits (23, 25, 30, 37–45). By phenotypically studying *Kcne5*$^{-/0}$ mice, we discovered that Kcne5 regulates $K_V2.1$ current ($I_{K,slow,2}$) (27, 29) in mouse ventricles. Furthermore, we demonstrated region- and myocyte-subtype–specific differences in the ventricular role of Kcne5, observing that *Kcne5* deletion augments $I_{K,slow,1}$ (generated by $K_V1.5$) (in addition to $I_{Kslow,2}$) in the apex but not the septum. Previously, we found that *Kcne2* deletion downregulates ventricular $I_{Kslow,2}$ by hampering $K_V1.5$ trafficking to the ICDs (30). We also found that, despite not being expressed in mouse heart, *Kcne3* deletion predisposes to ventricular arrhythmias and AF *via* an autoimmune attack on the adrenal glands that increases serum aldosterone (19, 23). In the atria, this tendency was demonstrated to occur *via* increased $K_V1.5$

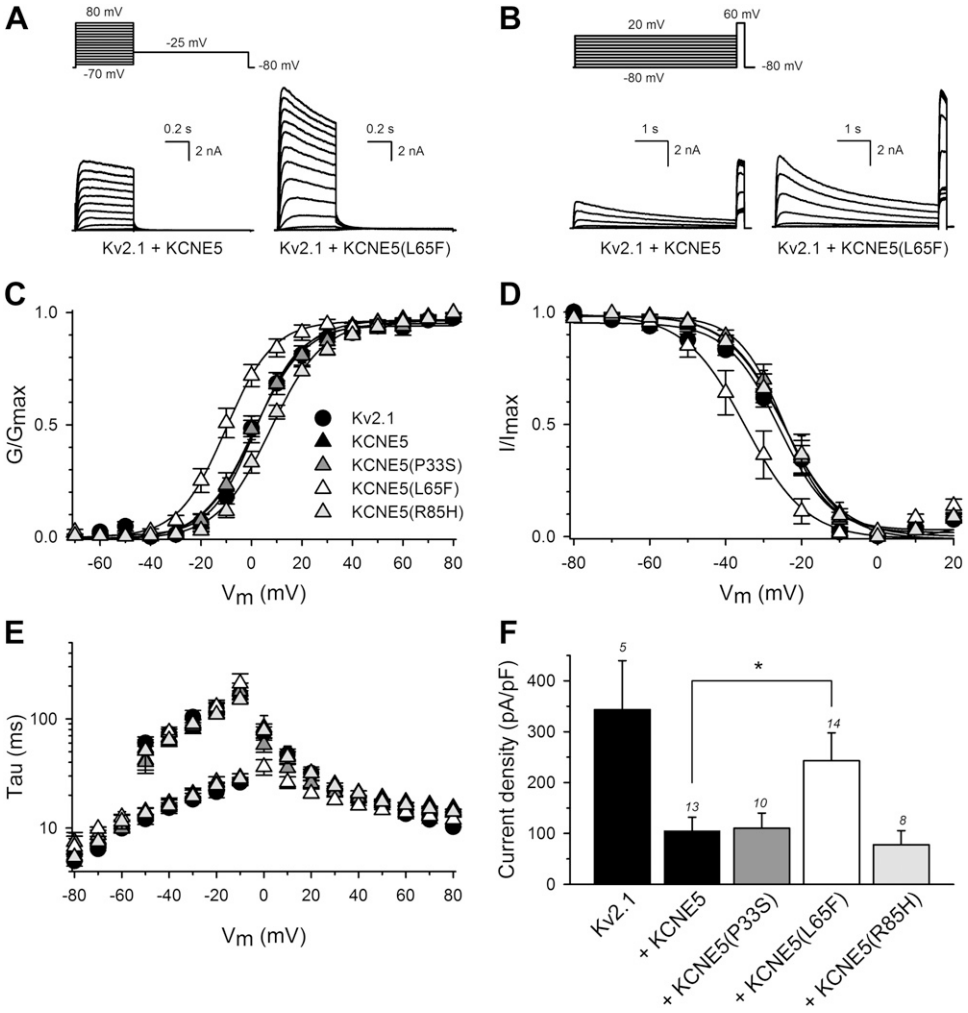

Figure 8. AF-associated KCNE5-L65F causes a gain-of-function of $K_V2.1$-KCNE5 channels. *A–D*) Biophysical properties of $K_V2.1$ coexpressed with WT or mutant human KCNE5. All recordings were performed on cells from 3 to 5 repeated transfections of 2–5 independent cell cultures. Representative current recordings determined the activation (*A*) and inactivation (*B*) properties of $K_V2.1$+KCNE5 and $K_V2.1$+KCNE5-L65F. The applied pulse protocols are given on top. Voltage-dependence of activation (*C*) and of inactivation (*D*) of $K_V2.1$+KCNE5, $K_V2.1$+KCNE5-P33S, $K_V2.1$+KCNE5-L65F, and $K_V2.1$+KCNE5-R85H. Activation and inactivation curves were obtained by plotting the normalized current amplitudes at −25 and +60 mV as a function of the 500-ms and 5-s prepulse potentials, respectively. Solid lines: Boltzmann fits. Coexpression of KCNE5-L65F shifted both the voltage dependence of activation and of inactivation. $P < 0.05$. *E*) Time constants of activation and deactivation of $K_V2.1$ coexpressed with KCNE5 variants as indicated; symbols as in *C*. Activation and deactivation constants were derived from single and double exponential fits of the raw current recordings, respectively. *F*) Current densities at 0 mV of $K_V2.1$ coexpressed with KCNE5 variants, as indicated. The numbers above each bar represent the number of cells analyzed. The L65F mutation increased current density compared with WT $K_V2.1$-KCNE5 channels. $*P < 0.05$.

recycling, leading again to diminished $I_{Kslow,2}$ (19). Future studies will focus on elucidating the mechanism for KCNE5 modulation of $K_V1.5$ current density.

In the present study, *Kcne5* deletion increased $I_{to,f}$ density, but the change was less dramatic than we observed for $I_{K,slow}$ and was also restricted to the apical myocytes, despite the known capacity for KCNE5 to robustly regulate K_V4 channels *in vitro* (15, 46, 47). This finding, together with the apical-specific $I_{K,slow,1}$ regulation by KCNE5 suggests that myocyte subtype-specific mechanisms are in place to limit $K_V\alpha$ subunit regulation by KCNE5, despite its capacity to interact in other cell subtypes or contexts.

Our finding that *Kcne5* is expressed in both atria and ventricles in mice is congruent with our expression data for human cardiac tissue, where we identified KCNE5 throughout the human heart, in line with prior studies (5–7), with slightly raised expression in the atria. We also detected Kcne5 protein expression specifically at the ventricular ICDs. We observed neither cardiac hypertrophy nor $K_V\alpha$ subunit transcript remodeling in $Kcne5^{-/0}$ mice, suggesting that the arrhythmias we detected by intracardiac ECG arose primarily from a purely electrical defect.

Our findings are the first, to our knowledge, to demonstrate β-subunit regulation of $K_V2.1$ in mice, and the augmentation of $I_{K,slow}$ arising from *Kcne5* deletion is consistent with current knowledge of the mechanistic bases for human AF and BrS (*i.e.*, pathologic increase in specific K_V currents; the more common basis for BrS is loss of function of voltage-gated sodium channels, but gain in K_V current has a similar effect). The relatively subtle and apically restricted effect of *Kcne5* deletion on $I_{to,f}$ in mouse ventricles is of interest, given that Ohno and colleagues (15) reported that BrS-linked *KCNE5* mutants increase the current conducted by human K_V4 channels. K_V4 channels may be regulated differently with respect to KCNEs in mouse *vs.* human hearts, with more extensive modulation in the latter. Alternatively, the capacity of KCNE5 mutants to alter K_V4-KCNE5 channel function *in vitro* may not be representative of the primary molecular mechanism underlying human BrS disease pathogenesis. In the mouse model presented herein, *Kcne5* deletion gave rise to specific

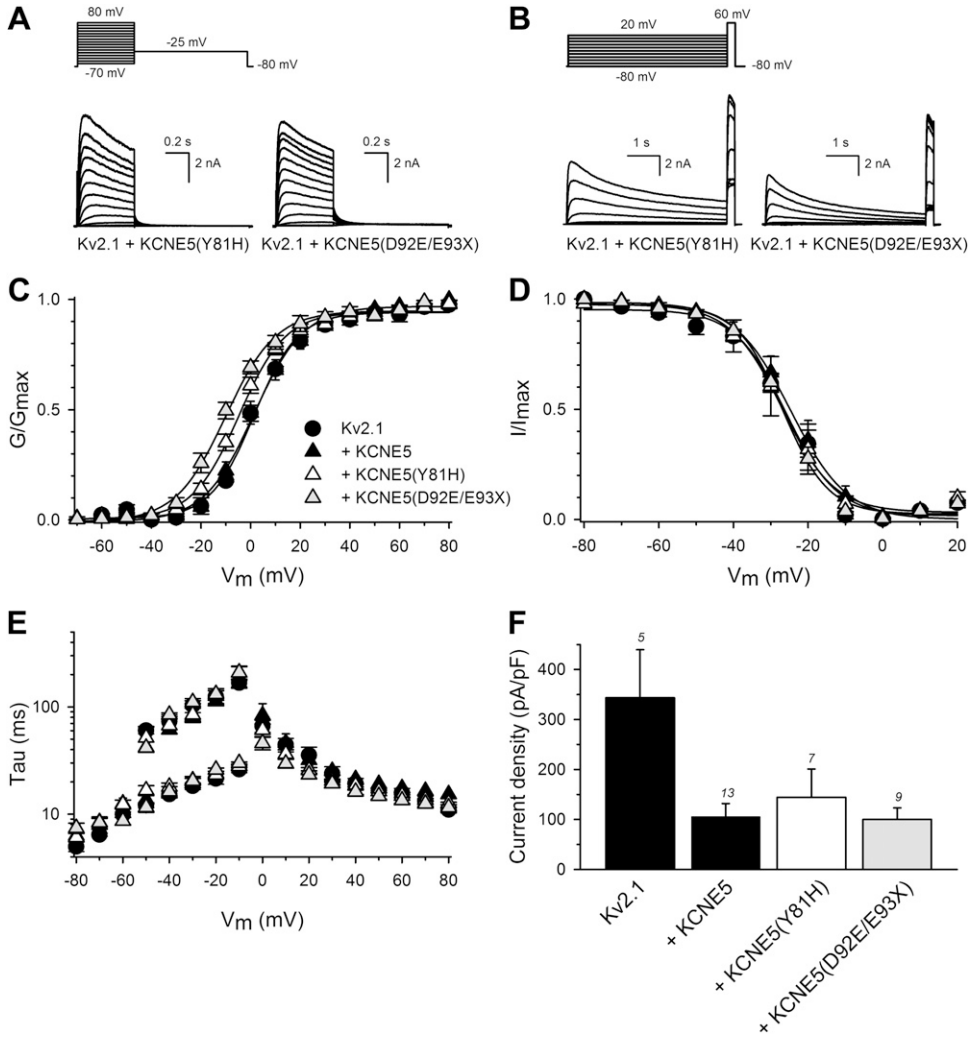

Figure 9. BrS-associated KCNE5 mutations cause a negative shift in the voltage dependence of $K_V2.1$-KCNE5 channels. All recordings were performed on cells from 3 to 5 repeated transfections of 2–5 independent cell cultures *A–D*) Biophysical properties of $K_V2.1$ coexpressed with WT or mutant human KCNE5. Representative current recordings determined the activation (*A*) and inactivation (*B*) properties of $K_V2.1$+KCNE5-Y81H and $K_V2.1$+KCNE5- D92E/E93X. The applied pulse protocols are given on top. Voltage-dependence of activation (*C*) and of inactivation (*D*) of $K_V2.1$+KCNE5, $K_V2.1$+KCNE5-Y81H, and $K_V2.1$+KCNE5- D92E/E93X. Activation and inactivation curves were obtained as in Fig. 4. Solid lines: the Boltzmann fits. Coexpression of KCNE5-D92E/E93X shifted the voltage dependence of activation. $P < 0.05$. *E*) Time constants of activation and deactivation of $K_V2.1$ coexpressed with KCNE5 variants as indicated; symbols as in *C*. Activation and deactivation constants as in Fig. 4*E*. *F*) Current densities at 0 mV of $K_V2.1$ coexpressed with KCNE5 variants as indicated. The numbers above each bar represent the number of analyzed cells.

K_V current augmentation, and macroscopically caused VPBs, which were followed by postextrasystolic compensatory pauses and in one case, a spontaneous polymorphic VT. Thus, as is thought to occur in human BrS, augmentation of specific K_V currents in mice *via Kcne5* disruption caused ventricular arrhythmia.

Our data present strong evidence of a novel KCNE5-$K_V2.1$ interaction in mouse cardiac myocytes; however, little is known about how these subunits interact. Expression of the subunits in HL-1 cells revealed that neither subunit affected the trafficking or localization of the other; however, our electrophysiology data suggest that KCNE5 directly regulates $K_V2.1$ channel attributes at the plasma membrane, in line with our previous work in HEK293 cells (20). We detected most of both human and mouse KCNE5 in dense

TABLE 2. *Biophysical properties of human $K_V2.1$ alone or coexpressed with WT or mutant human KCNE5*

	Activation				Inactivation			Deactivation		
Subunits	$V_{1/2}$	k	τ (at +60 mV)	n	$V_{1/2}$	k	n	$\tau 1$ (at −40 mV)	$\tau 2$ (at −40 mV)	n
$K_V2.1$	0.0 ± 1.9	9.4 ± 0.5	15.7 ± 1.6	6	−26.5 ± 1.6	5.2 ± 0.5	5	15.3 ± 1.1	73.1 ± 11.1	4
$K_V2.1$+										
WT	1.3 ± 2.2	9.7 ± 0.7	17.4 ± 0.9	7	−24.3 ± 2.8	5.7 ± 0.2	8	15.6 ± 1.0	61.4 ± 5.1	8
P33S	−0.2 ± 2.5	10.0 ± 1.1	16.0 ± 1.2	6	−23.9 ± 2.1	5.6 ± 0.4	6	16.2 ± 2.6	68.0 ± 7.6	5
L65F	−10.4 ± 2.4	9.1 ± 1.3	13.9 ± 1.1	7	−34.8 ± 3.3	5.6 ± 0.2	7	17.0 ± 1.1	75.3 ± 5.2	4
R85H	7.0 ± 1.8	10.4 ± 1.0	16.4 ± 0.7	6	−24.1 ± 2.4	6.4 ± 0.3	6	16.0 ± 1.1	63.9 ± 7.7	5
Y81H	−2.4 ± 2.1	9.6 ± 0.6	14.8 ± 0.3	6	−26.9 ± 3.9	5.4 ± 0.3	5	18.0 ± 1.5	67.2 ± 10.7	6
D92E/E93X	−5.2 ± 1.4	8.8 ± 0.5	13.4 ± 0.9	7	−26.4 ± 1.3	5.8 ± 0.3	5	16.3 ± 1.8	84.4 ± 3.5	5

Values are means ± SEM. $V_{1/2}$, midpoint (mV) of activation or inactivation; k, slope factor; τ, time constant (ms); n, number of cells. Values underlined showed a statistically significant difference compared to $K_V2.1$+KCNE5 values. $P < 0.05$.

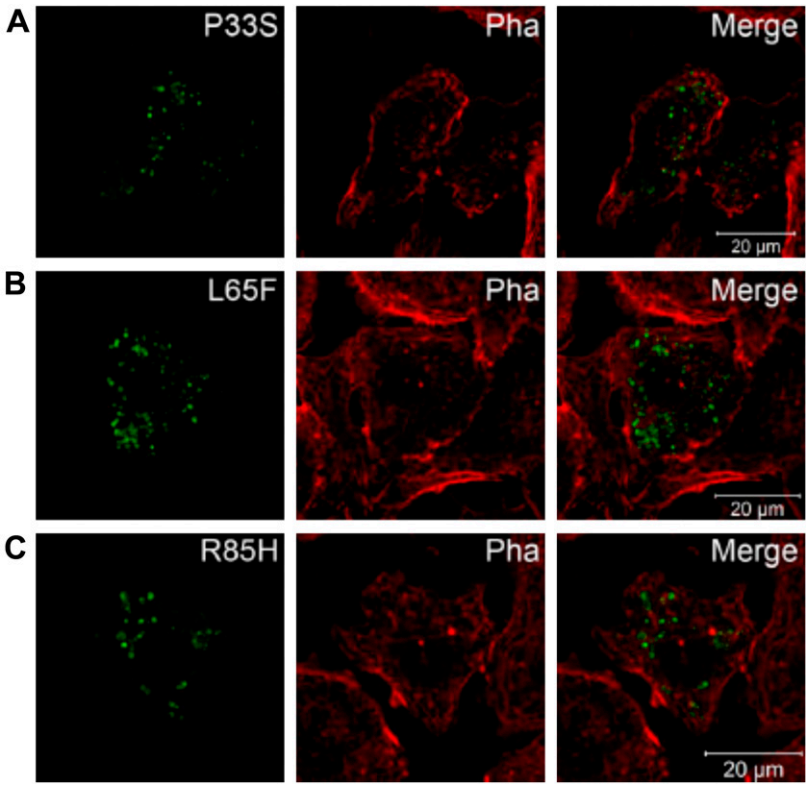

Figure 10. AF-associated KCNE5 mutants locate similarly to WT KCNE5 in HL-1 cells. KCNE5-P33S (*A*), KCNE5-L65F (*B*), and KCNE5-R85H (*C*) expressed in HL-1 cells alone were found in compartments similar to WT KCNE5 (compare to Fig. 6) visualized with confocal microcopy. Thus, the mutations did not seem to confer a trafficking deficiency. Phalloidin (Pha) was used to mark the cell membrane.

clusters at the membrane and in some intracellular clusters and vesicles located in proximity to the lysosomal marker LAMP2. $K_V2.1$ was mainly located at the border of the cell, overlapping the cell membrane marker phalloidin, but could also be found in vesicular structures similar to KCNE5. We speculate that some of the intracellular compartments positive for KCNE5 subunits are compartments of the late endosomal pathway and could serve either as a recycling reserve or as part of an endocytic mechanism regulating the number of $K_V2.1$ channels at the membrane. These observations are in line with results obtained in HEK293 cells (18). In this model, *Kcne5* deletion would prevent this recycling, thereby contributing to augmentation of $K_V2.1$ current density. A similar model could apply to other channels inhibited by KCNE5.

Finally, in our study, KCNE5-L65F lacked the inhibitory effect on $K_V2.1$ exhibited by WT KCNE5 and shifted the voltage dependence of activation and inactivation to more negative potentials. To date, no native current within the human heart has been assigned to $K_V2.1$, yet both $K_V2.1$ mRNA and protein have been detected in human ventricles and atria (33, 34). Ravn *et al.* (16) speculated that the L65F mutation in KCNE5 is associated with nonfamilial or acquired forms of AF, given that it causes a gain-of-function of I_{Ks}. Our findings, at the very least, suggest mechanistic commonalties between KCNE5 regulation of $K_V7.1$ and $K_V2.1$ and the possibility that human KCNE5-linked AF is more complex than first thought and perhaps involves $K_V2.1$, a channel of which little is known in terms of its importance in the human heart.

CONCLUSIONS

We provide the first description of the physiologic roles of KCNE5 *in vivo*. Mouse *Kcne5* functions as a ventricular myocyte subtype-specific inhibitor of $I_{Kslow,1}$ and I_{Kslow2}, which are conducted by $K_V1.5$ and $K_V2.1$, respectively, and to a lesser extent $I_{to,f}$ (K_V4 α subunits). *Kcne5* deletion increases ventricular arrhythmia susceptibility. These findings provide potential mechanistic clues to the molecular basis of human KCNE5-linked BrS and AF. FJ

ACKNOWLEDGMENTS

The authors thank Dr. Morten Thomsen [University of Copenhagen (UCPH), Copenhagen, Denmark] for advice on mouse ECG analysis and the Core Facility for Integrated Microscopy at UCPH. This work was supported by a framework grant of the Danish National Research Foundation (to N.S.); a Ph.D. stipend from the Faculty of Health and Medical Sciences, UCPH (to J.-P.D.); funding from the Arvid Nilsson Foundation (to J.-P.D.); the People Programme (Marie Curie Actions) of the European Union's Seventh Framework Programme Grant FP7/2007–2013 (Research Executive Agency Grant Agreement 608765) and a grant from the Lundbeck Foundation (to T.A.J.); a postdoctoral fellowship from the Research Foundation–Flanders (FWO) (to E.B.); and U.S. National Institutes of Health/National Heart, Lung and Blood

Institute Grant HL079275 and Postdoctoral Diversity Supplement Grant HL079275-S1 (to G.W.A.). The authors declare no conflicts of interest.

AUTHOR CONTRIBUTIONS

J.-P. David, U. Lisewski, T. K. Roepke, N. Schmitt, and G. W. Abbott designed the research; J.-P. David, U. Lisewski, S. M. Crump, T. A. Jepps, E. Bocksteins, N. Wilck, and J. Lossie performed the research; J.-P. David, U. Lisewski, S. M. Crump, T. A. Jepps, E. Bocksteins, N. Wilck, J. Lossie, and G. W. Abbott analyzed the data; and J.-P. David, S. M. Crump, T. A. Jepps, E. Bocksteins, T. K. Roepke, N. Schmitt, and G. W. Abbott wrote the manuscript.

REFERENCES

1. Abbott, G. W. (2015) The KCNE2 K^+ channel regulatory subunit: ubiquitous influence, complex pathobiology. *Gene* **569**, 162–172
2. Abbott, G. W. (2016) KCNE1 and KCNE3: the yin and yang of voltage-gated K(+) channel regulation. *Gene* **576**, 1–13
3. Abbott, G. W. (2016) KCNE4 and KCNE5: K(+) channel regulation and cardiac arrhythmogenesis. *Gene* **593**, 249–260
4. McCrossan, Z. A., and Abbott, G. W. (2004) The minK-related peptides. *Neuropharmacology* **47**, 787–821
5. Bendahhou, S., Marionneau, C., Haurogne, K., Larroque, M. M., Derand, R., Szuts, V., Escande, D., Demolombe, S., and Barhanin, J. (2005) In vitro molecular interactions and distribution of KCNE family with KCNQ1 in the human heart. *Cardiovasc. Res.* **67**, 529–538
6. Gaborit, N., Le Bouter, S., Szuts, V., Varro, A., Escande, D., Nattel, S., and Demolombe, S. (2007) Regional and tissue specific transcript signatures of ion channel genes in the non-diseased human heart. *J. Physiol.* **582**, 675–693
7. Lundquist, A. L., Manderfield, L. J., Vanoye, C. G., Rogers, C. S., Donahue, B. S., Chang, P. A., Drinkwater, D. C., Murray, K. T., and George, A. L., Jr. (2005) Expression of multiple KCNE genes in human heart may enable variable modulation of I(Ks). *J. Mol. Cell. Cardiol.* **38**, 277–287
8. Crump, S. M., and Abbott, G. W. (2014) Arrhythmogenic KCNE gene variants: current knowledge and future challenges. *Front. Genet.* **5**, 3
9. Barhanin, J., Lesage, F., Guillemare, E., Fink, M., Lazdunski, M., and Romey, G. (1996) K(V)LQT1 and lsK (minK) proteins associate to form the I(Ks) cardiac potassium current. *Nature* **384**, 78–80
10. Sanguinetti, M. C., Curran, M. E., Zou, A., Shen, J., Spector, P. S., Atkinson, D. L., and Keating, M. T. (1996) Coassembly of K(V)LQT1 and minK (IsK) proteins to form cardiac I(Ks) potassium channel. *Nature* **384**, 80–83
11. Schmitt, N., Grunnet, M., and Olesen, S. P. (2014) Cardiac potassium channel subtypes: new roles in repolarization and arrhythmia. *Physiol. Rev.* **94**, 609–653
12. Piccini, M., Vitelli, F., Seri, M., Galietta, L. J., Moran, O., Bulfone, A., Banfi, S., Pober, B., and Renieri, A. (1999) KCNE1-like gene is deleted in AMME contiguous gene syndrome: identification and characterization of the human and mouse homologs. *Genomics* **60**, 251–257
13. Jonsson, J. J., Renieri, A., Gallagher, P. G., Kashtan, C. E., Cherniske, E. M., Bruttini, M., Piccini, M., Vitelli, F., Ballabio, A., and Pober, B. R. (1998) Alport syndrome, mental retardation, midface hypoplasia, and elliptocytosis: a new X linked contiguous gene deletion syndrome? *J. Med. Genet.* **35**, 273–278
14. Lane, W., Robson, M., Lowry, R. B., and Leung, A. K. (1994) X-linked recessive nephritis with mental retardation, sensorineural hearing loss, and macrocephaly. *Clin. Genet.* **45**, 314–317
15. Ohno, S., Zankov, D. P., Ding, W. G., Itoh, H., Makiyama, T., Doi, T., Shizuta, S., Hattori, T., Miyamoto, A., Naiki, N., Hancox, J. C., Matsuura, H., and Horie, M. (2011) KCNE5 (KCNE1L) variants are novel modulators of Brugada syndrome and idiopathic ventricular fibrillation. *Circ. Arrhythm Electrophysiol.* **4**, 352–361
16. Ravn, L. S., Aizawa, Y., Pollevick, G. D., Hofman-Bang, J., Cordeiro, J. M., Dixen, U., Jensen, G., Wu, Y., Burashnikov, E., Haunso, S., Guerchicoff, A., Hu, D., Svendsen, J. H., Christiansen, M., and Antzelevitch, C. (2008) Gain of function in IKs secondary to a mutation in KCNE5 associated with atrial fibrillation. *Heart Rhythm* **5**, 427–435
17. Ravn, L. S., Hofman-Bang, J., Dixen, U., Larsen, S. O., Jensen, G., Haunsø, S., Svendsen, J. H., and Christiansen, M. (2005) Relation of 97T polymorphism in KCNE5 to risk of atrial fibrillation. *Am. J. Cardiol.* **96**, 405–407
18. David, J. P., Stas, J. I., Schmitt, N., and Bocksteins, E. (2015) Auxiliary KCNE subunits modulate both homotetrameric Kv2. 1 and heterotetrameric Kv2.1/Kv6.4 channels. *Sci. Rep.* **5**, 12813
19. Lisewski, U., Koehncke, C., Wilck, N., Buschmeyer, B., Pieske, B., and Roepke, T. K. (2016) Increased aldosterone-dependent Kv1.5 recycling predisposes to pacing-induced atrial fibrillation in Kcne3$^{-/-}$ mice. *FASEB J.* **30**, 2476–2489
20. Soltysinska, E., Olesen, S. P., Christ, T., Wettwer, E., Varró, A., Grunnet, M., and Jespersen, T. (2009) Transmural expression of ion channels and transporters in human nondiseased and end-stage failing hearts. *Pflugers Arch.* **459**, 11–23
21. Vandesompele, J., De Preter, K., Pattyn, F., Poppe, B., Van Roy, N., De Paepe, A., and Speleman, F. (2002) Accurate normalization of real-time quantitative RT-PCR data by geometric averaging of multiple internal control genes. *Genome Biol.* **3**, RESEARCH0034
22. Livak, K. J., and Schmittgen, T. D. (2001) Analysis of relative gene expression data using real-time quantitative PCR and the 2 (-Delta Delta C(T)) method. *Methods* **25**, 402–408
23. Hu, Z., Crump, S. M., Anand, M., Kant, R., Levi, R., and Abbott, G. W. (2014) Kcne3 deletion initiates extracardiac arrhythmogenesis in mice. *FASEB J.* **28**, 935–945
24. David, J. P., Andersen, M. N., Olesen, S. P., Rasmussen, H. B., and Schmitt, N. (2013) Trafficking of the IKs-complex in MDCK cells: site of subunit assembly and determinants of polarized localization. *Traffic* **14**, 399–411
25. Roepke, T. K., King, E. C., Reyna-Neyra, A., Paroder, M., Purtell, K., Koba, W., Fine, E., Lerner, D. J., Carrasco, N., and Abbott, G. W. (2009) Kcne2 deletion uncovers its crucial role in thyroid hormone biosynthesis. *Nat. Med.* **15**, 1186–1194
26. Xu, H., Guo, W., and Nerbonne, J. M. (1999) Four kinetically distinct depolarization-activated K+ currents in adult mouse ventricular myocytes. *J. Gen. Physiol.* **113**, 661–678
27. Bou-Abboud, E., Li, H., and Nerbonne, J. M. (2000) Molecular diversity of the repolarizing voltage-gated K+ currents in mouse atrial cells. *J. Physiol.* **529**, 345–358
28. London, B., Jeron, A., Zhou, J., Buckett, P., Han, X., Mitchell, G. F., and Koren, G. (1998) Long QT and ventricular arrhythmias in transgenic mice expressing the N terminus and first transmembrane segment of a voltage-gated potassium channel. *Proc. Natl. Acad. Sci. USA* **95**, 2926–2931
29. Zhou, J., Kodirov, S., Murata, M., Buckett, P. D., Nerbonne, J. M., and Koren, G. (2003) Regional upregulation of Kv2.1-encoded current, IK,slow2, in Kv1DN mice is abolished by crossbreeding with Kv2DN mice. *Am. J. Physiol. Heart Circ. Physiol.* **284**, H491–H500
30. Roepke, T. K., Kontogeorgis, A., Ovanez, C., Xu, X., Young, J. B., Purtell, K., Goldstein, P. A., Christini, D. J., Peters, N. S., Akar, F. G., Gutstein, D. E., Lerner, D. J., and Abbott, G. W. (2008) Targeted deletion of kcne2 impairs ventricular repolarization via disruption of I(K,slow1) and I(to,f). *FASEB J.* **22**, 3648–3660
31. McCrossan, Z. A., Roepke, T. K., Lewis, A., Panaghie, G., and Abbott, G. W. (2009) Regulation of the Kv2.1 potassium channel by minK and MiRP1. *J. Membr. Biol.* **228**, 1–14
32. O'Connell, K. M., Whitesell, J. D., and Tamkun, M. M. (2008) Localization and mobility of the delayed-rectifer K+ channel Kv2.1 in adult cardiomyocytes. *Am. J. Physiol. Heart Circ. Physiol.* **294**, H229–H237
33. Kääb, S., Dixon, J., Duc, J., Ashen, D., Näbauer, M., Beuckelmann, D. J., Steinbeck, G., McKinnon, D., and Tomaselli, G. F. (1998) Molecular basis of transient outward potassium current downregulation in human heart failure: a

decrease in Kv4.3 mRNA correlates with a reduction in current density. *Circulation* **98**, 1383–1393
34. Van Wagoner, D. R., Pond, A. L., McCarthy, P. M., Trimmer, J. S., and Nerbonne, J. M. (1997) Outward K+ current densities and Kv1.5 expression are reduced in chronic human atrial fibrillation. *Circ. Res.* **80**, 772–781
35. Olesen, M. S., Andreasen, L., Jabbari, J., Refsgaard, L., Haunsø, S., Olesen, S. P., Nielsen, J. B., Schmitt, N., and Svendsen, J. H. (2014) Very early-onset lone atrial fibrillation patients have a high prevalence of rare variants in genes previously associated with atrial fibrillation. *Heart Rhythm* **11**, 246–251
36. Claycomb, W. C., Lanson, N. A., Jr., Stallworth, B. S., Egeland, D. B., Delcarpio, J. B., Bahinski, A., and Izzo, N. J., Jr. (1998) HL-1 cells: a cardiac muscle cell line that contracts and retains phenotypic characteristics of the adult cardiomyocyte. *Proc. Natl. Acad. Sci. USA* **95**, 2979–2984
37. Abbott, G. W., and Jepps, T. A. (2016) Kcne4 deletion sex-dependently alters vascular reactivity. *J. Vasc. Res.* **53**, 138–148
38. Crump, S. M., Hu, Z., Kant, R., Levy, D. I., Goldstein, S. A., and Abbott, G. W. (2016) Kcne4 deletion sex- and age-specifically impairs cardiac repolarization in mice. *FASEB J.* **30**, 360–369
39. Hu, Z., Kant, R., Anand, M., King, E. C., Krogh-Madsen, T., Christini, D. J., and Abbott, G. W. (2014) Kcne2 deletion creates a multisystem syndrome predisposing to sudden cardiac death. *Circ. Cardiovasc. Genet.* **7**, 33–42
40. Hu, Z., Wei, W., Zhou, L., Chen, M., and Abbott, G. W. (2018) Kcne4 deletion sex-specifically predisposes to cardiac arrhythmia via testosterone-dependent impairment of RISK/SAFE pathway induction in aged mice. *Sci. Rep.* **8**, 8258
41. Lee, S. M., Baik, J., Nguyen, D., Nguyen, V., Liu, S., Hu, Z., and Abbott, G. W. (2017) *Kcne2* deletion impairs insulin secretion and causes type 2 diabetes mellitus. *FASEB J.* **31**, 2674–2685
42. Lee, S. M., Nguyen, D., Anand, M., Kant, R., Köhncke, C., Lisewski, U., Roepke, T. K., Hu, Z., and Abbott, G. W. (2016) Kcne2 deletion causes early-onset nonalcoholic fatty liver disease via iron deficiency anemia. *Sci. Rep.* **6**, 23118
43. Drici, M. D., Arrighi, I., Chouabe, C., Mann, J. R., Lazdunski, M., Romey, G., and Barhanin, J. (1998) Involvement of IsK-associated K+ channel in heart rate control of repolarization in a murine engineered model of Jervell and Lange-Nielsen syndrome. *Circ. Res.* **83**, 95–102
44. Vetter, D. E., Mann, J. R., Wangemann, P., Liu, J., McLaughlin, K. J., Lesage, F., Marcus, D. C., Lazdunski, M., Heinemann, S. F., and Barhanin, J. (1996) Inner ear defects induced by null mutation of the isk gene. *Neuron* **17**, 1251–1264
45. Warth, R., and Barhanin, J. (2002) The multifaceted phenotype of the knockout mouse for the KCNE1 potassium channel gene. *Am. J. Physiol. Regul. Integr. Comp. Physiol.* **282**, R639–R648
46. Radicke, S., Cotella, D., Graf, E. M., Banse, U., Jost, N., Varró, A., Tseng, G. N., Ravens, U., and Wettwer, E. (2006) Functional modulation of the transient outward current Ito by KCNE beta-subunits and regional distribution in human non-failing and failing hearts. *Cardiovasc. Res.* **71**, 695–703
47. Abbott, G. W. (2017) β subunits functionally differentiate human Kv4.3 potassium channel splice variants. *Front. Physiol.* **8**, 66

Received for publication March 15, 2018.
Accepted for publication September 10, 2018.